Research article

JHEP|Reports

Macrophage ATG16L1 promotes liver regeneration after partial hepatectomy

Authors

Xinyu Zhan, Yan Bai, Qing Zhu, …, Zeyu Zhu, Zhuqing Rao, Haoming Zhou

Correspondence

zhuqingrao@njmu.edu.cn (Z. Rao), hmzhou@njmu.edu.cn (H. Zhou).

Graphical abstract

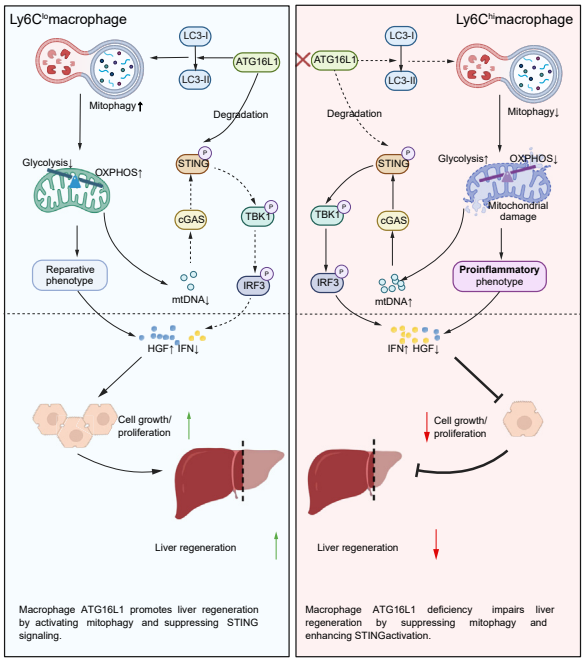

Highlights:

- ATG16L1 expression is increased after partial hepatectomy.
- Macrophage-specific *ATG16L1* deletion impairs liver regeneration.
- *ATG16L1* deletion remodels macrophage phenotypes by inhibiting mitophagy.
- Macrophage *ATG16L1* deletion inhibits liver regeneration by promoting and sustaining cGAS–STING pathway activation.
- Targeted activation of ATG16L1 promotes liver regeneration.

Impact and implications:

The autophagy-related gene *ATG16L1* mediates mitophagy, facilitating the clearance of damaged mitochondria in macrophages following partial hepatectomy and maintaining a reparative macrophage phenotype. ATG16L1 deficiency triggers excessive STING activation and inhibits its degradation, thereby suppressing liver regeneration. Thus, targeting ATG16L1 in macrophages could represent a novel strategy to promote liver regeneration.

https://doi.org/10.1016/j.jhepr.2025.101330

Research article

JHEP|Reports

Macrophage ATG16L1 promotes liver regeneration after partial hepatectomy

Xinyu Zhan[1,2,3,†], **Yan Bai**[4,†], **Qing Zhu**[4,†], Yiyun Gao[1,2,3], Fan Li[1,2,3], Qingfa Bu[5], Zeyu Zhu[1,2,3], Zhuqing Rao[4,*], Haoming Zhou[1,2,3,*]

JHEP Reports **2025**. vol. 7 | 1–19

Background & Aims: Autophagy plays an important role in liver regeneration. However, most studies are limited to hepatocytes, and the function and mechanism of macrophage autophagy in liver regeneration remain unclear. This study investigated the role of the essential autophagy gene encoding autophagy-related 16-like 1 (*ATG16L1*), which regulates the macrophage phenotype in liver regeneration.

Methods: We generated *FloxP-Atg16l1* (*Atg16l1*$^{FL/FL}$), *Lyz2-Cre Atg16l1* knockout (KO) (*Atg16l1*$^{M\text{-}KO}$), and myeloid-specific *Atg16l1-overexpression*-knock-in (*Atg16l1*^{OE}) mice. These mice were subjected to 70% partial hepatectomy to demonstrate the role of ATG16L1 in macrophages during liver regeneration.

Results: ATG16L1 expression was significantly upregulated in macrophages during the early stages of liver regeneration. ATG16L1 deletion in macrophages substantially delayed liver regeneration in mice and caused a marked imbalance in Ly6C^{hi} and Ly6C^{lo} macrophage proportions in the liver. RNA-sequencing analysis revealed that, compared with macrophages isolated from *Atg16l1*$^{FL/FL}$ mice, those from *Atg16l1*$^{M\text{-}KO}$ mice exhibited significant downregulation of genes associated with oxidative phosphorylation and upregulation of proinflammatory gene expression. Mechanistically, ATG16L1 loss impaired mitophagy in macrophages, leading to the accumulation of mitochondrial damage and a metabolic shift that promoted proinflammatory macrophage polarization. ATG16L1 deficiency not only promoted macrophage mitochondrial (mt)DNA release and cyclic GMP-AMP synthase–stimulator of interferon genes (STING) activation, but also suppressed STING degradation. Sustained STING hyperactivation and subsequent increased release of downstream interferons further contributed to the inhibition of liver regeneration. Notably, pharmacological activation or genetic overexpression of ATG16L1 significantly enhanced liver regeneration in mice.

Conclusions: ATG16L1 has a pivotal role in liver regeneration by affecting the phenotype and function of macrophages. Thus, targeting ATG16L1 in macrophages could present a novel strategy for promoting liver regeneration.

Introduction

Liver regeneration can occur following various types of injury caused by drugs, toxins, and surgeries, but the extent of that regeneration directly affects patient prognosis.[1] The strong regenerative ability of the liver is crucial for ensuring functional compensation and recovery in patients following liver resection.[2] However, clinical cases of liver failure resulting from insufficient compensatory capacity of the remaining liver following major liver resection, such as hemihepatectomy or living-donor liver transplantation, are not uncommon.[3] Factors such as hepatitis virus infection and liver cirrhosis can impair liver reserve function and its regenerative and reparative abilities. Therefore, in-depth research into the specific cellular and molecular mechanisms regulating liver regeneration and repair is essential for enhancing the regenerative capacity of liver and improving patient outcomes.

Liver regeneration is an organized dynamic process primarily involving nonparenchymal cells in addition to the proliferation of liver parenchymal cells. Macrophages are not only crucial for maintaining liver homeostasis, but also have a role in liver pathology; thus, their role in liver regeneration and repair has gained increasing attention.[4] For example, recent studies showed that macrophages are heterogeneous in both origin and function. Infiltrating macrophages involved in regulating regeneration and repair are often classified into two categories based on their Ly6C expression levels: classically activated proinflammatory macrophages (Ly6C^{hi}) and alternatively activated reparative macrophages (Ly6C^{lo}). Both types can have dual roles in either inhibiting or promoting liver regeneration and repair. Therefore, ensuring a coordinated balance between these two macrophage phenotypes is vital.[5] Furthermore, Ly6C^{hi} macrophages can transition to Ly6C^{lo} macrophages

* Corresponding author. Address: Hepatobiliary Center, The First Affiliated Hospital of Nanjing Medical University, 300 Guang Zhou Road, Nanjing, 210029, Jiangsu, China (H. Zhou); and Department of Anesthesiology, Jiangsu Province People's Hospital and Nanjing Medical University First Affiliated Hospital, Nanjing, 210029, China (Z. Rao).
E-mail addresses: zhuqingrao@njmu.edu.cn (Z. Rao), hmzhou@njmu.edu.cn (H. Zhou).
† These authors share co-first authorship.
https://doi.org/10.1016/j.jhepr.2025.101330

during regeneration;[6,7] however, the specific mechanisms involved remain unclear.

Liver regeneration requires sufficient energy and cellular materials for DNA replication and cell division. As a recycling mechanism that maintains homeostasis in eukaryotic cells, autophagy has an important role in providing energy and substrates during regeneration. A positive synergistic effect has been demonstrated between autophagy and hepatocyte proliferation.[8] However, whether autophagy activation occurs in nonparenchymal cells, particularly macrophages, during regeneration and whether these cells rely on autophagic changes to perform their respective functions remain unclear.

Autophagy related 16-like 1 (ATG16L1) is a key mediator in the lipidation of LC3 and the formation of autophagosomes during autophagy.[9] It not only coordinates intestinal epithelial cell homeostasis, but also has an active role in lipid metabolism in hepatocytes. Previously, we reported that *ATG16L1* deletion in macrophages exacerbated liver lipid accumulation and inflammation, ultimately promoting the progression of metabolic dysfunction-associated steatohepatitis.[10] However, the specific role of macrophage ATG16L1 in liver regeneration following partial hepatectomy (PHx) remains unclear.

In this study, we elucidated the molecular mechanisms by which ATG16L1 signaling regulates macrophage activation, hepatocyte proliferation, and intrahepatic inflammation during liver regenerative repair. We focused on the intrinsic links among autophagy, the reshaping of reparative macrophage phenotypes, and hepatocyte proliferation, thereby providing a theoretical foundation and potential therapeutic targets for the orderly regulation of liver regeneration and repair in clinical settings.

Materials and methods

Mice

The wild-type (WT), *FloxP-Atg16l1* (*Atg16l1*$^{FL/FL}$), *Lyz2-Cre Atg16l1* knockout (KO) (*Atg16l1*$^{M\text{-}KO}$), and myeloid-specific *Atg16l1-overexpression*-knock-in (*Atg16l1*^{OE}) mice used in this study were obtained from GemPharmatech Co (Nanjing, Jiangsu, China)., Ltd. The *FloxP-Tmem173* (*Tmem173*$^{FL/FL}$) and *Lyz2-Cre Tmem173* KO (*Tmem173*$^{M\text{-}KO}$) mice were provided by Shanghai Model Organisms Center, Inc. (Shanghai, China) All mouse strains had a C57BL/6J genetic background, were housed under specific pathogen-free conditions, were maintained on a 12-h light/dark cycle, and had free access to water and standard chow. All animals were treated humanely, and all procedures were approved by the Institutional Animal Care and Use Committee (IACUC:2304026) of Nanjing Medical University.

Methods

All methods and materials used in the study are detailed in the supplementary data online.

Data analysis

All data are presented as the mean ± SEM of at least three biological replicates per group. Two-tailed student's *t* test was applied for comparisons of two groups and one-way analysis of variance (ANOVA) for comparisons of more than two groups. $p < 0.05$ was considered statistically significant.

Results

Significant upregulation of ATG16L1 expression after PHx

To investigate ATG16L1 expression during liver regeneration, we established a mouse model of 70% PHx. After PHx, we measured the expression of ATG16L1 at different time points. Notably, ATG16L1 protein and mRNA levels in the mouse liver peaked at 48 h post PHx before declining, eventually returning to baseline levels at 7 days post PHx (Fig. 1A,B). To further confirm ATG16L1 expression in hepatic macrophages in the regenerative environment, we used western blot and quantitative (q)PCR. ATG16L1 expression in macrophages was significantly elevated after PHx, showing a synchronous pattern with the overall hepatic expression of ATG16L1 (Fig. 1C,D). Dual immunofluorescence staining further confirmed that ATG16L1 expression was upregulated in both hepatocytes and macrophages following PHx (Fig. 1E). In addition, the expression of autophagy-related genes, including *ATG5*, *ATG12*, and *Beclin*, was elevated after PHx (Fig. S1). These results indicate that ATG16L1 expression is upregulated in liver tissue after PHx, with a synchronized expression trend between hepatocytes and hepatic macrophages. Peak ATG16L1 expression coincides with the peak period of hepatocyte proliferation.[11] Moreover, *ATG5*, *ATG12*, and *Beclin* are also upregulated in macrophages.

Macrophage-specific *ATG16L1* deletion impairs liver regeneration

To further elucidate the potential role of macrophage-specific ATG16L1 during liver regeneration, we generated *Lyz2-Cre Atg16l1*-KO mice and performed hepatectomy on A*tg16l1*$^{M\text{-}KO}$ and *Atg16l1*$^{FL/FL}$ mice. Before PHx, there were no differences between the two groups of mice in terms of average body weight, liver weight, or liver lipid accumulation (Figs. S2A and B). However, compared with *Atg16l1*$^{FL/FL}$ mice, *Atg16l1*$^{M\text{-}KO}$ mice subjected to 90% PHx exhibited reduced tolerance to liver resection surgery and a significantly increased mortality rate (Fig. 2A). In the 70% PHx model, the liver-to-body weight ratio was lower in *Atg16l1*$^{M\text{-}KO}$ mice than in *Atg16l1*$^{FL/FL}$ mice at 48 h post PHx. However, no significant difference was observed between the two groups at 7 days post PHx (Fig. 2B), suggesting that the absence of ATG16L1 in macrophages leads to delayed recovery of liver mass. Furthermore, *Atg16l1*$^{M\text{-}KO}$ mice exhibited a significantly delayed decrease in liver enzyme levels, with serum alanine aminotransferase and aspartate aminotransferase levels remaining significantly higher than those in *Atg16l1*$^{FL/FL}$ mice between 12 and 72 h (Fig. 2C). We evaluated tissue injury at different time points using H&E staining and found no differences in injury between *Atg16l1*$^{FL/FL}$ and *Atg16l1*$^{M\text{-}KO}$ mice. Overall injury levels were also low in this model. This could be closely associated with delayed liver regeneration in these mice (Fig. 2D).

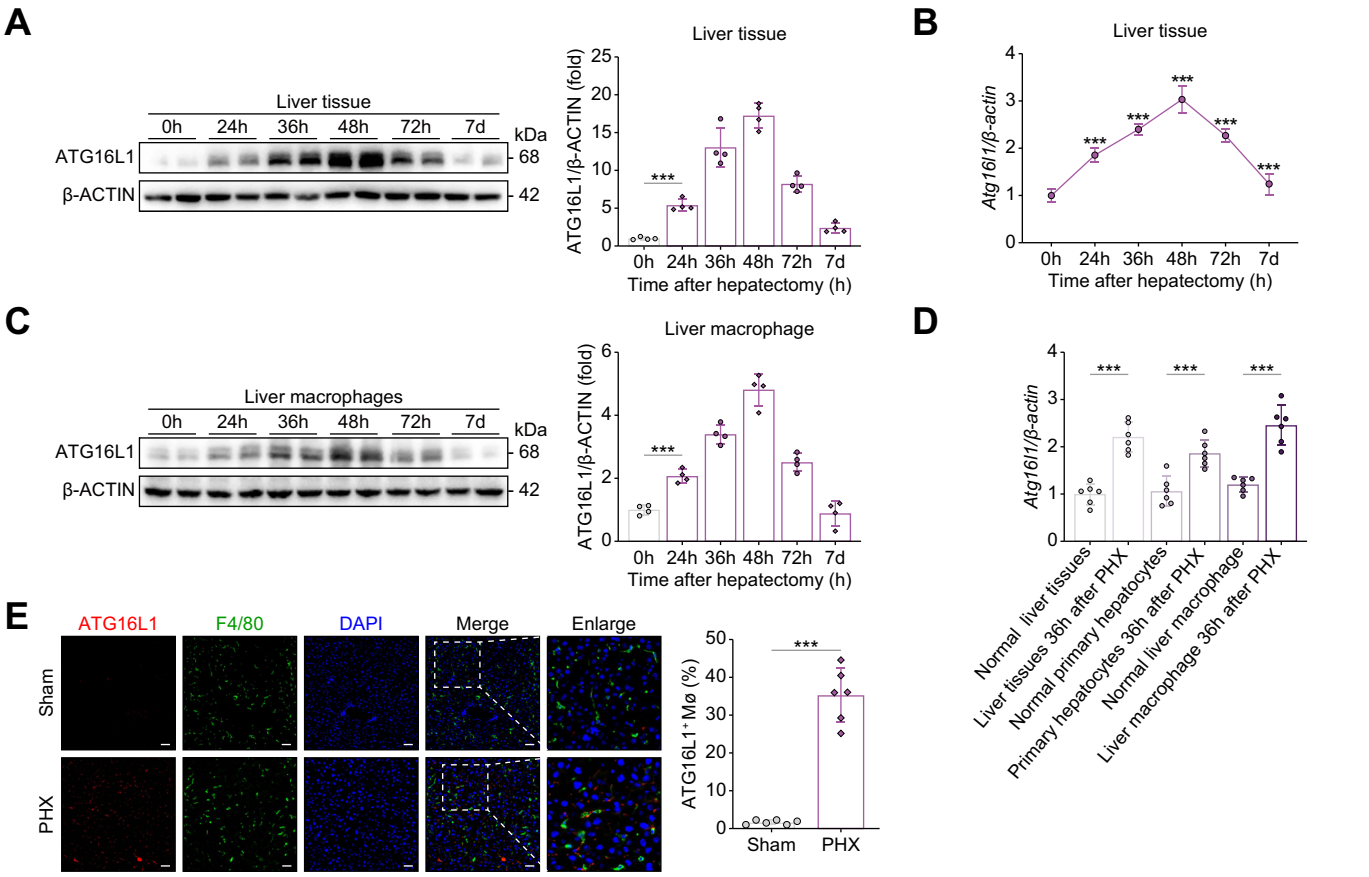

Fig. 1. ATG16L1 levels are significantly elevated in the mouse model after PHx. ATG16L1 protein (A) and mRNA (B) levels in mouse liver tissues at indicated time points post PHx (n = 4–6 per group). (C) Western blot analysis of ATG16L1 expression of liver macrophages at indicated time points post PHx (n = 4 per group). β-actin was used as a control. ***p <0.001, by one-way ANOVA with Bonferroni post-test. (D) Relative expression levels of *Atg16l1* mRNA in liver tissue, primary hepatocytes, and liver macrophages. ***p <0.001, by an unpaired, 2-tailed Student's t test. (E) Representative immunofluorescence co-staining images of ATG16L1 (red), F4/80 (green), and DAPI (blue) in mice and their quantification 36 h after PHx and in the sham group. Scale bar: 50 μm. ATG16L1, autophagy-related 1- like 1; PHx, partial hepatectomy.

According to immunohistochemistry staining for Ki67 and proliferating cell nuclear antigen, as well as western blot results, the overall proliferation level in *Atg16l1*$^{M\text{-}KO}$ mice was significantly lower than that in *Atg16l1*$^{FL/FL}$ mice at 36–72 h post surgery (Fig. 2E,F). Whole-liver sequencing further confirmed this finding because pathway enrichment analysis and qPCR results showed downregulation of the liver cell cycle pathway and significant reductions in the expression of the cell cycle markers Cyclin A2, Cyclin B1, Cyclin D1, and Cyclin E1, indicating a weakened G1–S phase transition in *Atg16l1*$^{M\text{-}KO}$ mice. The western blot results showed similar changes (Fig. 2G–I).

We supplemented these findings with an acute CCl4-induced liver injury model. At 36–72 h after CCl4 injection, both *Atg16l1*$^{M\text{-}KO}$ and *Atg16l1*$^{FL/FL}$ mice exhibited significant liver damage, with the damage being more severe in *Atg16l1*$^{M\text{-}KO}$ mice. Although liver injury in *Atg16l1*$^{FL/FL}$ mice was fully repaired 120 h after CCl4 injection, *Atg16l1*$^{M\text{-}KO}$ mice still displayed evident necrotic areas at 168 h post injection (Fig. S2C). Consistent with the PHx model results, expression of the proliferation marker Ki67 was significantly suppressed in the livers of *Atg16l1*$^{M\text{-}KO}$ mice (Fig. S2D). Taken together, these results suggest that *ATG16L1* deletion in macrophages delays hepatocyte proliferation after PHx.

Macrophage-specific *ATG16L1* deletion does not affect the initiation phase of liver regeneration after PHx

Macrophages contribute to the entire process of liver regeneration.[12] To determine whether the deletion of macrophage-specific *ATG16L1* delays liver regeneration by affecting the initiation phase, we first examined the gene expression of the cell cycle markers Cyclin A2, Cyclin B1, Cyclin D1, and Cyclin E1, as well as the protein levels of proliferating cell nuclear antigen, in liver tissue. No significant differences were observed between *Atg16l1*$^{M\text{-}KO}$ and *Atg16l1*$^{FL/FL}$ mice (Fig. 3A,B). Similarly, during the initiation phase, no notable difference was observed in the proportion of hepatic macrophages and neutrophils between the two groups (Fig. 3C,D).

Macrophage-derived IL-6 and tumor necrosis factor (TNF) are crucial cytokines in the initiation phase of liver regeneration.[13] Therefore, we compared the mRNA levels of IL-6 and TNF in liver tissue, as well as their serum concentrations during the early phase of regeneration. No significant differences were detected between the two groups (Fig. 3E,F). In addition, signal transducer and activator of transcription 3 (STAT3), a downstream signaling mediator in response to IL-6 and a key regulator of cell proliferation,[14] showed no difference in its active

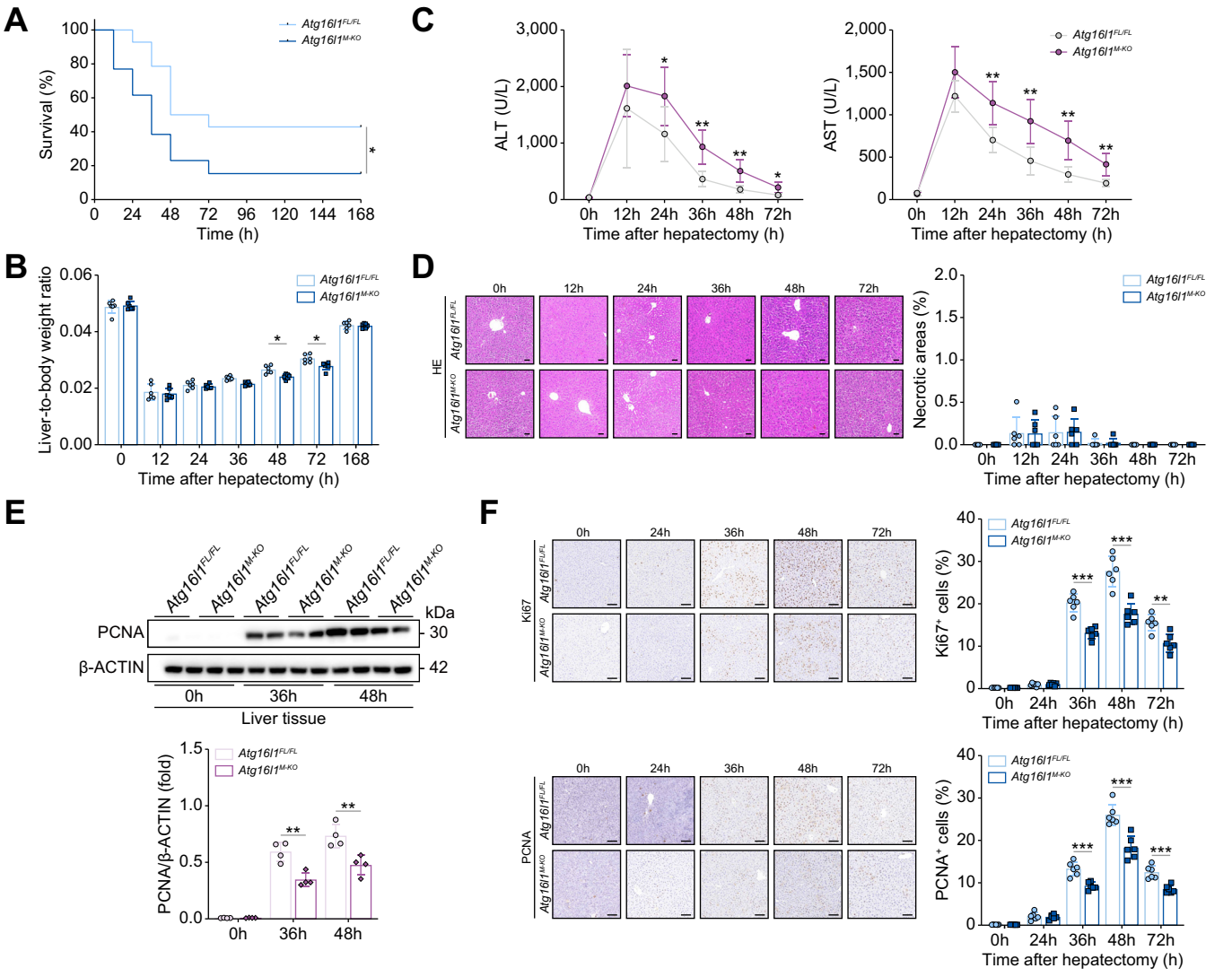

Fig. 2. Macrophage-specific ATG16L1 deletion inhibits hepatocyte proliferation during liver regeneration. (A) Survival curve of *Atg16l1*$^{FL/FL}$ and *Atg16l1*$^{M-KO}$ mice in response to lethal 90% PHx (n = 14 per group). (B) Liver-to-body weight ratio of *Atg16l1*$^{FL/FL}$ and *Atg16l1*$^{M-KO}$ mice at indicated time points after 70% PHx (n = 6 per group). (C) Serum ALT and AST levels assayed by ELISA at indicated time points post 70% PHx of *Atg16l1*$^{FL/FL}$ and *Atg16l1*$^{M-KO}$ mice. (D) Representative H&E staining and quantification of necrotic zones at indicated time points after PHx in *Atg16l1*$^{FL/FL}$ and *Atg16l1*$^{M-KO}$ mice (n = 6 per group). (E) Immunohistochemical staining of liver tissue for Ki67 and PCNA and their quantification at indicated time post 70% PHx in *Atg16l1*$^{FL/FL}$ and *Atg16l1*$^{M-KO}$ mice (n = 6 per group). (F) Western blot analysis and corresponding quantification of PCNA protein expression levels in mice liver tissue at different time points post PHx (n = 4 per group). β-actin was used as a control. (G) RNA-sequencing analysis of liver tissues at 36 h post PHx in mice. Bar chart showing the top-30 significantly expressed genes based on GO enrichment. The cell cycle signaling pathways ranked top for both their *p* values and count numbers. (H) Quantification of CyclinA2, CyclinB1, CyclinD1, and CyclinE1 mRNA expression in *Atg16l1*$^{FL/FL}$ and *Atg16l1*$^{M-KO}$ mice at different time points post PHx (n = 6 per group). (I) Western blot analysis and corresponding quantification of Cyclin A and Cyclin D1 expression levels in mice liver tissue at different time points post PHx (n = 4 per group). β-actin was used as a control.*p <0.05, **p <0.01, ***p <0.001, by two-way ANOVA with Bonferroni post-test. Scale bars: 50 μm (D), 100 μm (E). ALT, alanine aminotransferase; AST, aspartate aminotransferase; ATG16L1, autophagy-related 16-like 1; GO, Gene Ontology; KO, knockout; PCNA, proliferating cell nuclear antigen; PHx, partial hepatectomy.

form (phosphorylated STAT3) between *Atg16l1*$^{M-KO}$ and *Atg16l1*$^{FL/FL}$ mice (Fig. 3G). In summary, *ATG16L1* deletion in macrophages does not inhibit liver regeneration by affecting the initiation phase.

ATG16L1 deletion impairs liver regeneration by remodeling macrophage phenotypes

Hepatic macrophages can interact with other immune cell subsets to indirectly influence liver regeneration.[13,15] Therefore, we hypothesized that the loss of ATG16L1 in macrophages might lead to altered crosstalk with immune cells, affecting liver regeneration. We assessed post-PHx immune cell infiltration in the liver in both *Atg16l1*$^{M-KO}$ and *Atg16l1*$^{FL/FL}$ mice. Flow cytometry and immunohistochemistry revealed a significant increase in neutrophil infiltration in *Atg16l1*$^{M-KO}$ mice, with attenuated clearance of neutrophils during the regenerative phase (Fig. 4A,B). Recently, a collaboration between neutrophils and macrophages in coordinating inflammation and tissue repair was reported.[16] To investigate whether the inhibition of liver regeneration in ATG16L1-deficient macrophages is neutrophil dependent, we depleted neutrophils *in vivo* by administering Ly6G-specific antibodies and observed liver

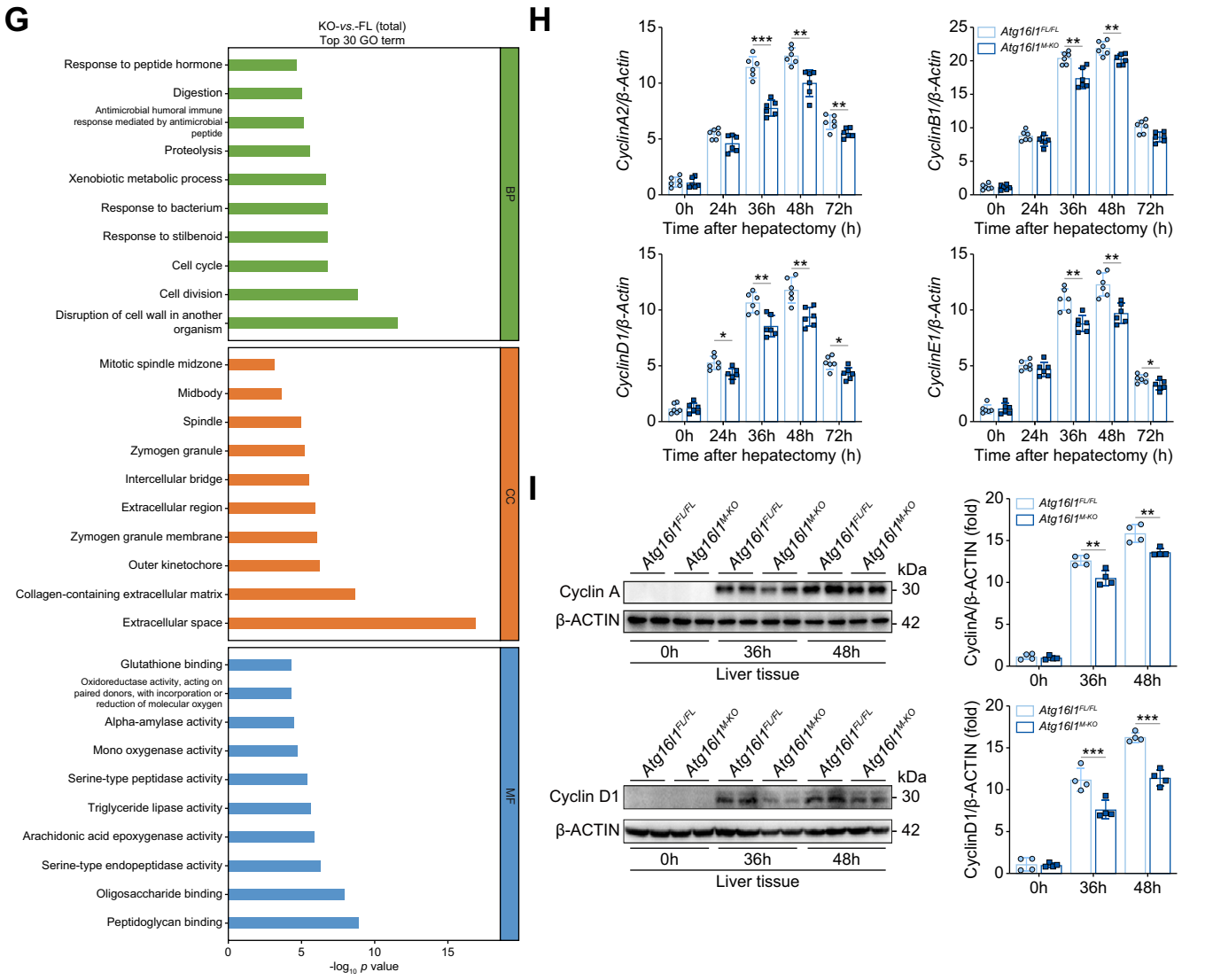

Fig. 2. (*continued*).

regeneration post PHx. Surprisingly, although neutrophil depletion delayed liver proliferation in both groups, hepatocyte proliferation at 36 h and 48 h post PHx remained significantly lower in *Atg16l1*$^{M\text{-}KO}$ mice than in *Atg16l1*$^{FL/FL}$ mice (Fig. 4C–E). This suggests that inhibition of liver regeneration caused by ATG16L1 deficiency in macrophages is not neutrophil dependent. Next, we examined the infiltration of natural killer cells (NK1.1^{hi}CD3^{-}), CD4^{+} T (CD3^{+}CD4^{+}), and CD8^{+} T (CD3^{+}CD8^{+}) cells. Flow cytometry results showed no significant differences in cell proportions or absolute numbers between the two groups (Fig. 4F).

These findings suggest that ATG16L1 influences liver regeneration by directly affecting macrophage phenotype transformation. Anti-F4/80 immunofluorescence staining revealed a significant increase in macrophage numbers in the liver of *Atg16l1*$^{M\text{-}KO}$ mice at 36 h post PHx (Fig. 5A). We further evaluated the hepatic macrophage population using flow cytometry. The results showed a shift toward monocyte-derived macrophages in *Atg16l1*$^{M\text{-}KO}$ mice, with a significant increase in the proportion of monocyte-derived macrophages and a relative decrease in Kupffer cells (KCs). Interestingly, although the proportion of KCs was significantly reduced, their absolute number showed no difference between the two groups (Fig. 5B).

Dual immunofluorescence staining showed that, at 36 h post PHx, 'M1-like' macrophages (iNOS^{+}F4/80^{+}) were significantly more abundant in the livers of *Atg16l1*$^{M\text{-}KO}$ mice than in those of *Atg16l1*$^{FL/FL}$ mice, whereas the number of 'M2-like' macrophages (CD206^{+}F4/80^{+}) was markedly reduced (Fig. 5C). In macrophage-mediated regeneration and repair studies, recruited reparative (M2-like) and proinflammatory (M1-like) macrophage subsets are often distinguished by Ly6C^{lo} and Ly6C^{hi} markers.[17,18] In the present study, *ATG16L1* deletion significantly altered the ratio of Ly6C^{lo} to Ly6C^{hi} macrophages. At 36 h post PHx, the proportion of Ly6C^{hi} macrophages in the livers of *Atg16l1*$^{M\text{-}KO}$ mice was significantly higher than that in *Atg16l1*$^{FL/FL}$ mice, whereas the proportion of Ly6C^{lo} macrophages was significantly reduced (Fig. 5D).

To clarify the impact of this change on hepatocyte proliferation, we co-cultured primary hepatocytes from WT mice

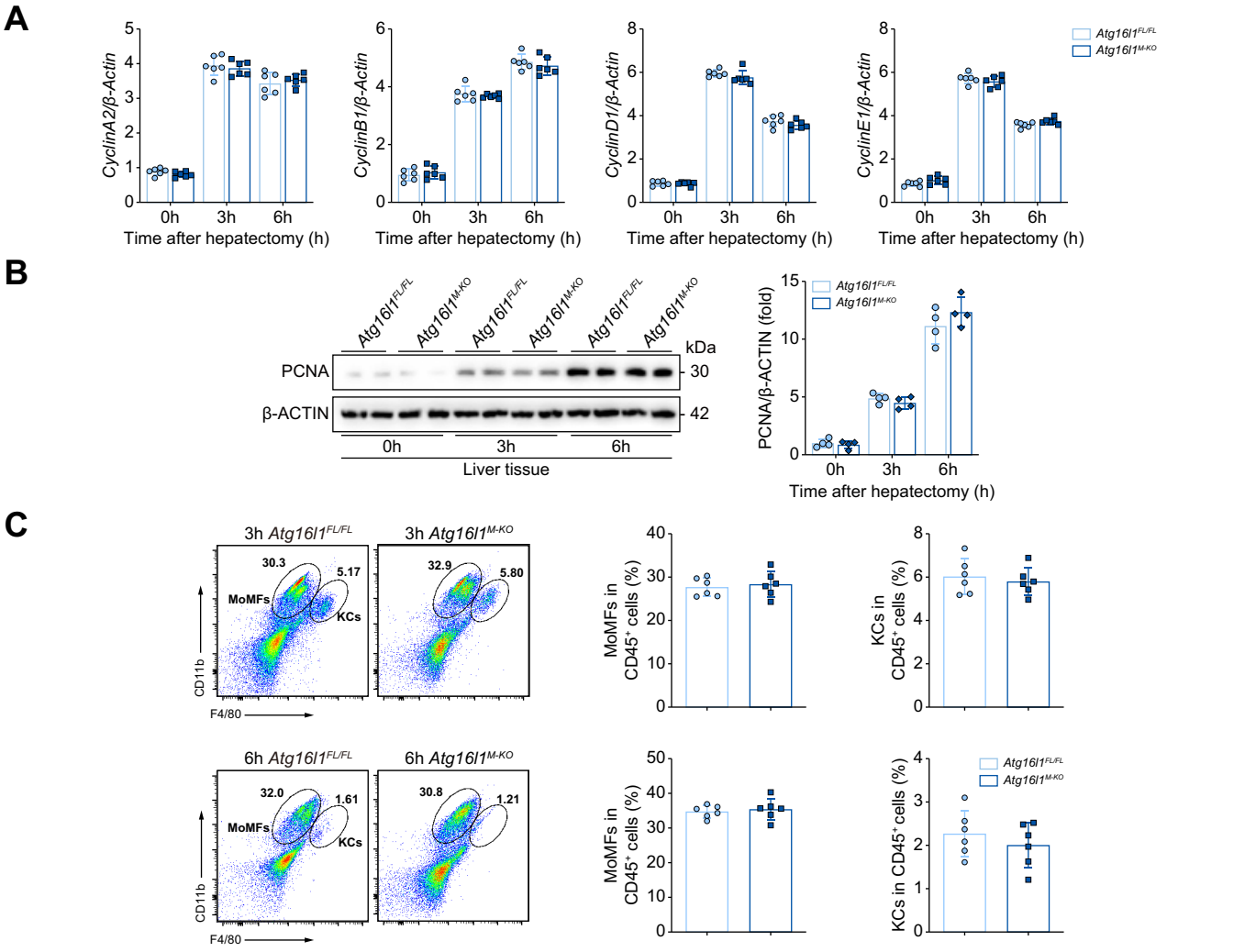

Fig. 3. Macrophage-specific ATG16L1 deletion does not influence the initiation phase of liver regeneration after PHx. (A) Quantification of CyclinA2, CyclinB1, CyclinD1, and CyclinE1 mRNA expression in *Atg16l1*$^{FL/FL}$ and *Atg16l1*$^{M\text{-}KO}$ mice 0–6 h after PHx (n = 6 per group). (B) Western blot analysis and corresponding quantification of PCNA expression in *Atg16l1*$^{FL/FL}$ and *Atg16l1*$^{M\text{-}KO}$ mice 0–6 h after PHx (n = 4 per group). NS, no significance, by two-way ANOVA with Bonferroni post-test. (C) Representative FACS plots and quantification of MoMFs and KCs in *Atg16l1*$^{FL/FL}$ and *Atg16l1*$^{M\text{-}KO}$ mice liver tissues 3 and 6 h after PHx (n = 6 per group). (D) Representative FACS plots and neutrophil quantification in *Atg16l1*$^{FL/FL}$ and *Atg16l1*$^{M\text{-}KO}$ mice liver tissues 3 and 6 h after PHx (n = 6 per group). NS, no significance, by an unpaired, 2-tailed Student's *t* test. (E) Quantification of IL-6 and TNF-α mRNA expression in *Atg16l1*$^{FL/FL}$ and *Atg16l1*$^{M\text{-}KO}$ mice at indicated time points after 70% PHx (n = 6 per group). (F) Serum IL-6 and TNF-α assayed by ELISA in *Atg16l1*$^{FL/FL}$ and *Atg16l1*$^{M\text{-}KO}$ mice 0, 3, and 6 h after 70% PHx (n = 6 per group). (G) Western blot analysis and corresponding quantification of STAT3 and p-STAT3 expression in *Atg16l1*$^{FL/FL}$ and *Atg16l1*$^{M\text{-}KO}$ mice. β-actin was used as a control. NS, no significance, by two-way ANOVA with Bonferroni post-test. ATG16L1, autophagy-related 16-like 1; KC, Kupffer cell; KO, knockout; MoMF, monocyte-derived macrophage; p-STAT3, phosphorylated signal transducer and activator of transcription 3; PCNA, proliferating cell nuclear antigen; PHx, partial hepatectomy; STAT3, signal transducer and activator of transcription 3; TNF, tumor necrosis factor.

with conditioned media from the macrophages of either *Atg16l1*$^{M\text{-}KO}$ or *Atg16l1*$^{FL/FL}$ mice for 48 h. We observed a significant reduction in the number of proliferating hepatocytes, as indicated by Ki67 staining, and a marked decrease in proliferating cell nuclear antigen protein levels in the *Atg16l1*$^{M\text{-}KO}$ group compared with those in the *Atg16l1*$^{FL/FL}$ group. Analysis of cytokine levels in the conditioned media showed significantly higher levels of proinflammatory cytokines, such as IL-1β, IL-6, and TNF, in the *Atg16l1*$^{M\text{-}KO}$ group, but a significantly lower level of hepatocyte growth factor (HGF), a key factor in promoting hepatocyte proliferation (Fig. 5E–H). Subsequently, we analyzed the gene expression profile of hepatic macrophages 36 h post PHx. RNA-sequencing analysis revealed that *ATG16L1* deletion led to significant upregulation of inflammation-related genes in macrophages, consistent with our earlier finding of a shift toward an 'M1-like' macrophage phenotype (Fig. 5I–K). In conclusion, macrophage-specific *ATG16L1* deletion disrupts the balance between proinflammatory and reparative macrophages following PHx, skewing the macrophage population toward a proinflammatory phenotype, which ultimately impairs liver regeneration.

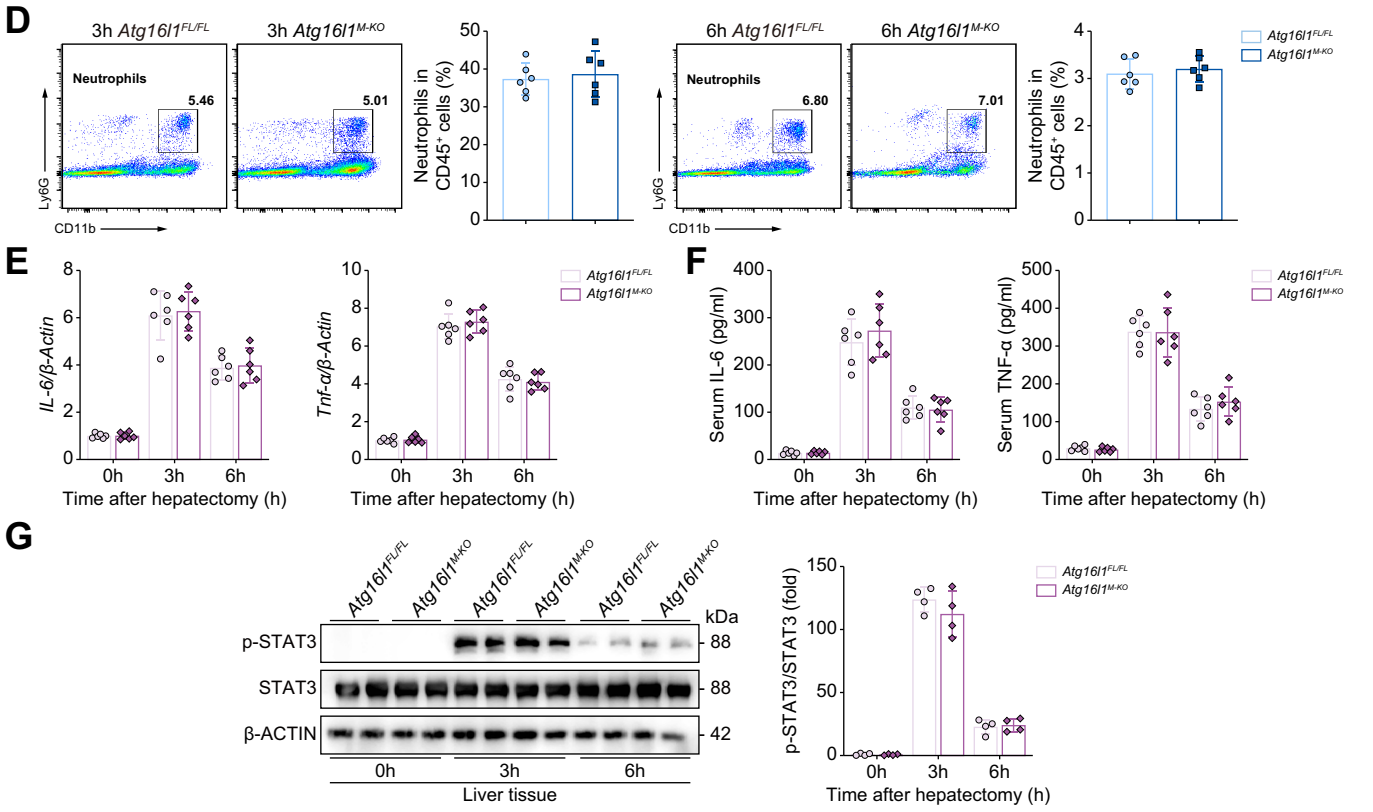

Fig. 3. (*continued*).

ATG16L1 deletion remodels macrophage phenotypes by inhibiting mitophagy

To investigate the mechanism underlying macrophage phenotype transformation, we performed Kyoto Encyclopedia of Genes and Genomes pathway and gene enrichment analyses. The results showed that the oxidative phosphorylation pathway in macrophages from *Atg16l1*$^{M\text{-}KO}$ mice had a significant *p* value, with related genes being significantly downregulated (Fig. 6A). Macrophage metabolism is crucial for shaping their phenotype: 'M1'-like macrophages rely on glycolysis, whereas 'M2'-like macrophages depend on mitochondria-driven oxidative phosphorylation.[19] Therefore, we introduced myeloid-specific *ATG16L1* overexpression mice to further explore the effect of ATG16L1 on macrophage metabolism. Specifically, we used the Seahorse XFe96 analyzer to assess mitochondrial metabolism and glycolysis in hepatic macrophages from *Atg16l1*$^{FL/FL}$, *Atg16l1*$^{M\text{-}KO}$, and *Atg16l1*^{OE} mice at 36 h post PHx. The results showed that *ATG16L1* deletion significantly promoted glycolysis in macrophages, whereas oxidative phosphorylation was markedly decreased. Conversely, *ATG16L1* overexpression enhanced mitochondrial metabolic activity and reduced glycolysis levels (Fig. 6B,C). Our experimental findings confirmed the regulatory role of ATG16L1 in macrophage metabolic pathways. Furthermore, we measured mitochondrial metabolic activity and glycolysis levels in Ly6C^{lo} and Ly6C^{hi} macrophages in WT mice at 36 h post PHx. We found that Ly6C^{lo} macrophages preferred oxidative phosphorylation, whereas Ly6C^{hi} macrophages were more inclined toward glycolysis (Figs. S3A and B). This further confirmed that ATG16L1 might alter the ratio of Ly6C^{lo} to Ly6C^{hi} macrophages in the liver after PHx by affecting macrophage metabolism.

Cellular metabolism depends on the structure and function of mitochondria.[20] Therefore, we examined mitochondrial function in hepatic macrophages at 36 h post PHx. In ATG16L1-deficient macrophages, we observed a reduction in mitochondrial membrane potential, an increase in mitochondrial reactive oxygen species (ROS) production, decreased glutathione (which represents the antioxidant level in mitochondria), and significantly elevated overall levels of cellular ROS. Conversely, ATG16L1 overexpression significantly improved mitochondrial function and reduced oxidative stress within the mitochondria (Fig. 6D–G).

Cellular electron microscopy results showed reduced mitochondrial electron density and edema in macrophages after liver resection. In the *Atg16l1*$^{M\text{-}KO}$ group, mitochondrial damage was more severe, with mitochondrial fragmentation and loss of intramitochondrial cristae, along with a significant reduction in the number of autophagosomes. By contrast, the *Atg16l1*^{OE} group exhibited better overall mitochondrial morphology and a significantly increased number of autophagosomes compared with the *Atg16l1*$^{FL/FL}$ group (Fig. 6H).

Given that *ATG16L1* is a key gene in the autophagy process,[9,21] we hypothesized that *ATG16L1* deletion might inhibit mitophagy in hepatic macrophages after PHx, leading to the accumulation of mitochondrial damage. Therefore, we conducted mitophagy assays. Double immunofluorescence staining for TOM20 and dsDNA revealed mtDNA leakage and accumulation in the cytoplasm of hepatic macrophages in both

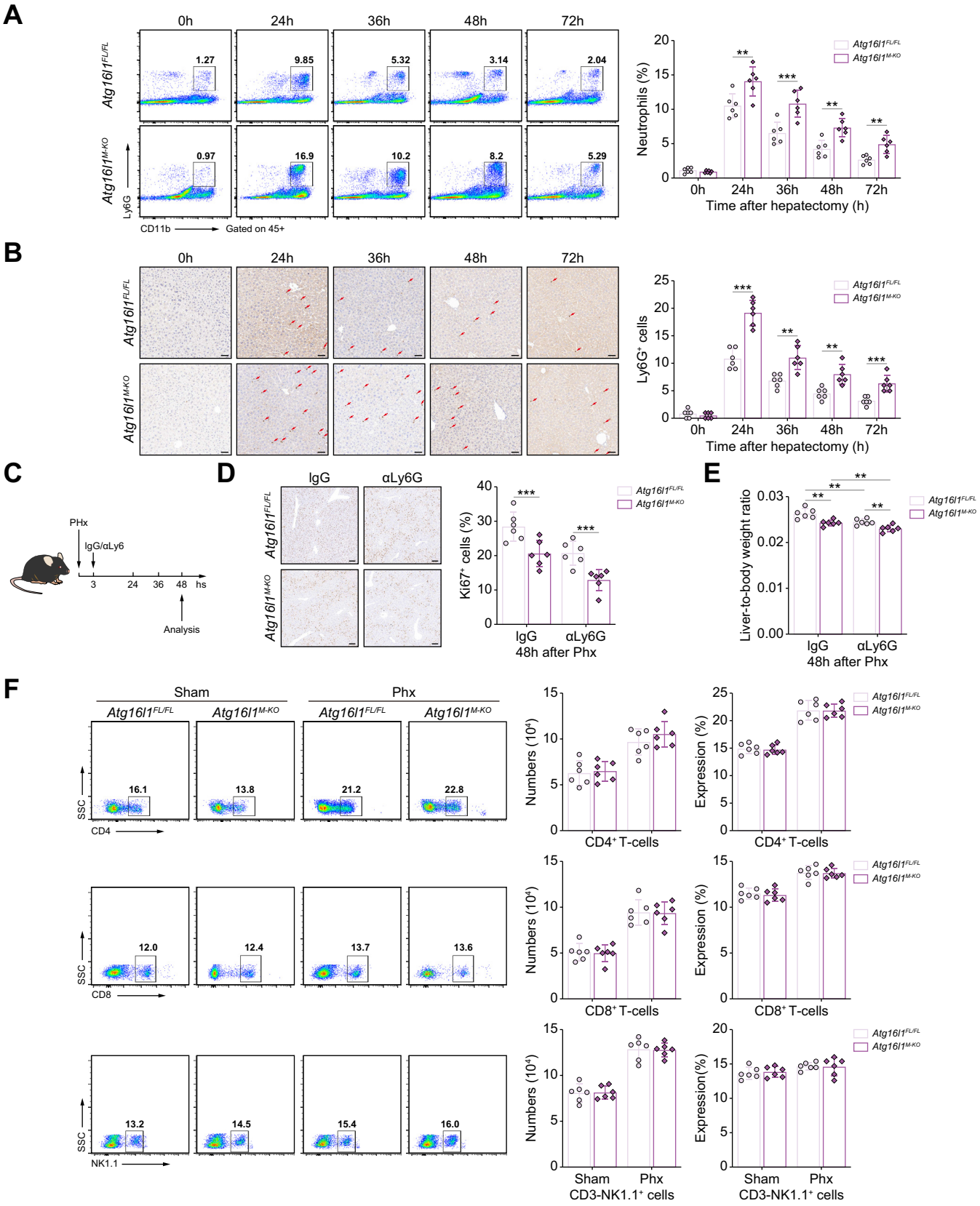

Fig. 4. Inhibition of liver regeneration by macrophage-specific ATG16L1 deletion is independent of other immune cells. (A) Representative FACS plots and neutrophil quantification of *Atg16l1*$^{FL/FL}$ and *Atg16l1*$^{M\text{-}KO}$ mice liver tissues at indicated time points after 70% PHx (n = 6 per group). (B) Representative immunohistochemical images and quantification of hepatic Ly6G^{+} cells in *Atg16l1*$^{FL/FL}$ and *Atg16l1*$^{M\text{-}KO}$ mice at indicated time points after 70% PHx (n = 6 per group). (C) Mice were treated with the neutrophil-depleting anti-Ly6G monoclonal antibody or an isotype control (IgG) 3 h after PHx. (D) Representative liver sections 48 h after PHx and

Atg16l1$^{FL/FL}$ and *Atg16l1*$^{M\text{-}KO}$ mice at 36 h post PHx, with more considerable mtDNA accumulation in *Atg16l1*$^{M\text{-}KO}$ macrophage cytoplasm. By contrast, mtDNA leakage was significantly reduced in *Atg16l1*^{OE} macrophage cytoplasm (Fig. 6I). We subsequently used qPCR to measure mtDNA/nuclear (n)DNA copy numbers and performed western blotting to detect several mitochondrial proteins, including TOM20, TIM23, and VDAC1, as well as the autophagy-related proteins P62 and LC3b. The results showed that *ATG16L1* deletion significantly inhibited the conversion of LC3b I to LC3b II, thereby blocking the occurrence of mitophagy. By contrast, *ATG16L1* overexpression significantly increased the mitophagy flux in macrophages (Fig. 6J,K).

To determine autophagic flux, we compared mice treated with leupeptin, a lysosomal inhibitor, with those without leupeptin treatment. Following PHx, the levels of LC3-II in hepatic macrophages of *Atg16l1*$^{FL/FL}$ and *Atg16l1*^{OE} mice were significantly elevated, and this increase was further augmented in the presence of leupeptin. However, this was not observed in the hepatic macrophages of *Atg16l1*$^{M\text{-}KO}$ mice, indicating that *ATG16L1* deletion impairs the lipidation process of LC3b-I, thereby inhibiting autophagy. Furthermore, changes in mitochondrial protein levels demonstrated that mitophagy was also suppressed (Fig. 6L). In summary, these results indicate that ATG16L1 can mitigate mitochondrial damage during liver regeneration by regulating mitophagy, thereby maintaining metabolic activity in macrophages and ultimately controlling the macrophage phenotype.

Macrophage ATG16L1 deletion inhibits liver regeneration by promoting and sustaining cGAS–STING pathway activation

Given that *ATG16L1* deletion induces macrophage metabolic phenotype shifts through mitochondrial damage, we hypothesized that other pathways may also inhibit liver regeneration. A previous study reported that *ATG16L1* deletion significantly enhances stimulator of interferon genes (STING) activity in intestinal epithelial cells.[22] Our earlier work revealed that defects of mitochondrial autophagy in macrophage senescence cause mtDNA leakage and activate the intracellular STING pathway.[23] Furthermore, interferon (IFN) can inhibit liver regeneration.[24] Therefore, we hypothesized that, after liver resection, STING in macrophages might act as a crucial mediator inhibiting liver regeneration in the context of ATG16L1 deficiency. We identified 18 genes involved in the IFN-I response from our sequencing data and validated their upregulation using qPCR. Interaction analysis using the STRING database indicated that the cyclic GMP-AMP synthase (cGAS)–STING pathway may be implicated in the response to ATG16L1 deletion (Fig. 7A–C).[25] Immunofluorescence staining of liver tissue showed a significant increase in phosphorylated (p)-STING^{+} macrophages in the liver of *Atg16l1*$^{M\text{-}KO}$ mice at 36 h post PHx, whereas p-STING expression in *Atg16l1*^{OE} macrophages was significantly reduced. Western blot analysis further confirmed that ATG16L1 deletion significantly upregulated the cGAS–STING signaling pathway in hepatic macrophages, whereas ATG16L1 overexpression markedly inhibited this pathway (Fig. 7D,E).

To further explore the role of STING pathway activation in liver regeneration after ATG16L1 deletion, we silenced STING using adeno-associated virus (AAV) vectors and analyzed liver regeneration post resection. The results showed partial recovery of liver regeneration and reduced serum inflammatory cytokine levels, particularly IFN, in STING-silenced *Atg16l1*$^{M\text{-}KO}$ mice compared with *Atg16l1*$^{M\text{-}KO}$ mice. Western blot analysis also revealed the downregulation of STING downstream signals, including p-TANK-binding kinase 1 (TBK1) and p-IFN regulatory factor 3 (IRF3), in hepatic macrophages (Fig. 7F–H). When primary hepatocytes from WT mice were cultured with conditioned media from the three groups of macrophages for 48 h, STING silencing in *Atg16l1*$^{M\text{-}KO}$ macrophages had a similar effect on hepatocyte proliferation to that observed *in vivo* (Fig. 7J,K). Next, we assessed mitochondrial metabolic activity and glycolysis levels in hepatic macrophages from the three groups of mice after PHx. Notably, STING silencing did not reverse the metabolic pathways in *Atg16l1*$^{M\text{-}KO}$ macrophages (Figs. S4A and B), which might be because of irreversible mitochondrial damage caused by ATG16L1 deficiency. Notably, when we performed PHx in *Tmem173*$^{FL/FL}$ and *Tmem173*$^{M\text{-}KO}$ mice, liver regeneration was enhanced in *Tmem173*$^{M\text{-}KO}$ mice compared with *Tmem173*$^{FL/FL}$ mice (Figs. S4C and D). These findings indicate that STING acts as a key mediator in the inhibition of liver regeneration following ATG16L1 deletion in macrophages.

ATG16L1 deficiency in BJ1 fibroblasts affects the degradation of STING pathway proteins.[26] Thus, we hypothesized that a similar phenomenon may occur in macrophages. We treated bone marrow-derived macrophages from *Atg16l1*$^{FL/FL}$, *Atg16l1*$^{M\text{-}KO}$, and *Atg16l1*^{OE} mice with the STING agonist DMXAA and examined the expression of p-STING, STING, p-TBK1, and TBK1 at different time points. Immunofluorescence and western blot results demonstrated that ATG16L1 deficiency inhibited the degradation of STING signaling proteins, promoting sustained activation of the pathway, whereas STING degradation was accelerated in ATG16L1-overexpressing macrophages (Figs. S5A and B). However, the precise mechanism by which ATG16L1 influences STING degradation requires further investigation. In summary, our findings suggest that macrophage ATG16L1 deficiency inhibits liver regeneration by promoting and sustaining STING pathway activation.

Targeted activation of ATG16L1 promotes liver regeneration

To confirm the role of macrophage ATG16L1 activation in liver regeneration, we extracted bone marrow-derived macrophages from *Atg16l1*$^{FL/FL}$, *Atg16l1*$^{M\text{-}KO}$, and *Atg16l1*^{OE} mice and implanted them into the spleens of WT mice undergoing PHx. At 36 h post PHx, we analyzed liver-to-body weight ratios and

respective quantification of Ki67-positive hepatocytes in *Atg16l1*$^{FL/FL}$ and *Atg16l1*$^{M\text{-}KO}$ mice (n = 6 per group). (E) Liver-to-body weight ratio of *Atg16l1*$^{FL/FL}$ and *Atg16l1*$^{M\text{-}KO}$ mice at 48 h after 70% PHx (n = 6 group). $^{**}p$ <0.01, $^{***}p$ <0.001, by two-way ANOVA with Bonferroni post-test. (F) Representative FACS plots of CD4^{+}T, CD8^{+}T, and NK cells from *Atg16l1*$^{FL/FL}$ and *Atg16l1*$^{M\text{-}KO}$ mice 36 h after PHx and quantification of the proportion and numbers in CD45^{+} cells (n = 6 per group). NS, no significance, by two-way ANOVA with Bonferroni post-test. Scale bars: 50 μm (B), 100 μm (D). ATG16L1, autophagy-related 16-like 1; KO, knockout; PHx, partial hepatectomy.

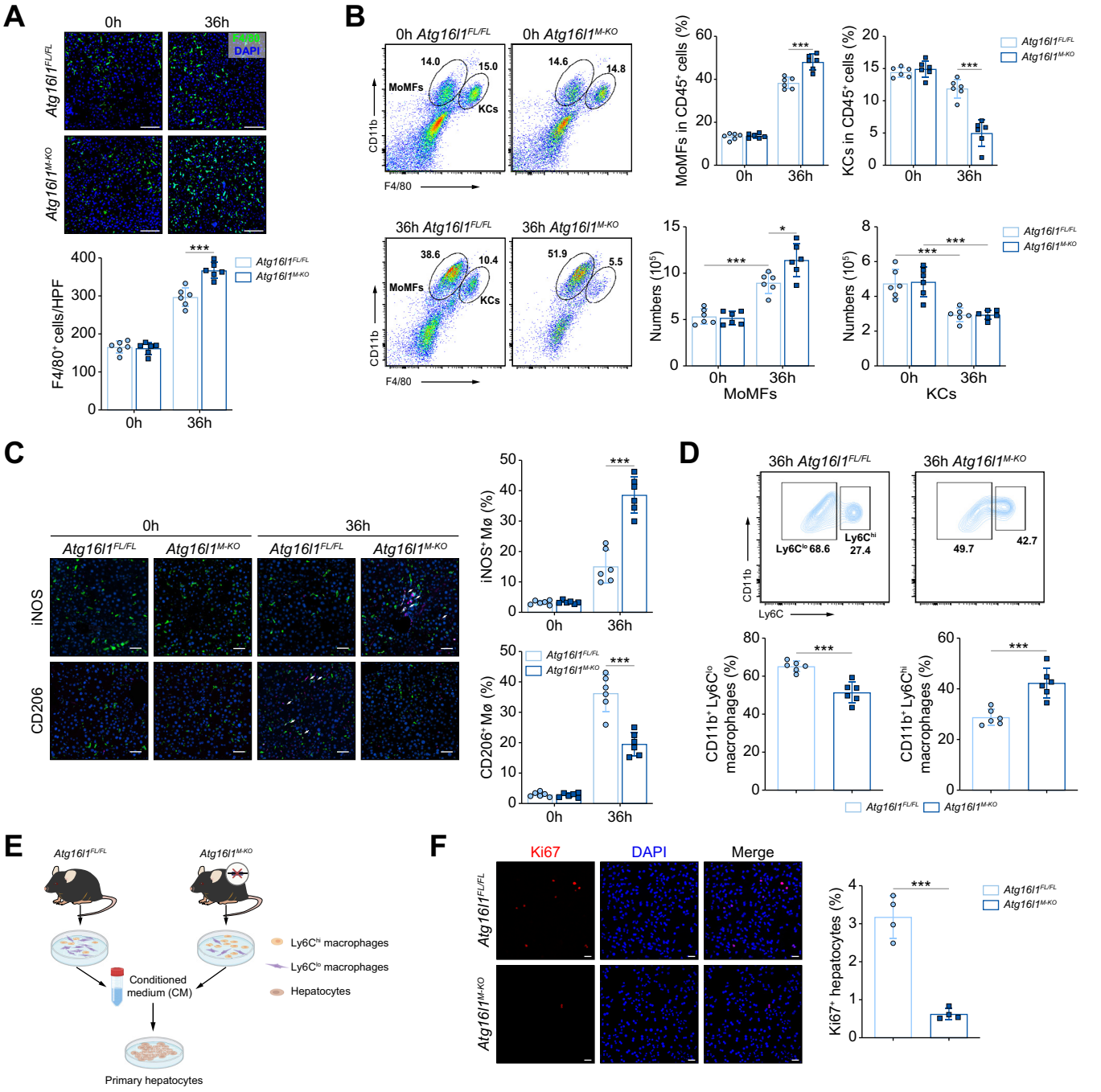

Fig. 5. ATG16L1 deletion affects liver regeneration by remodeling macrophage phenotypes. (A) Representative IF co-staining images of F4/80 (green) and DAPI (blue) in *Atg16l1*$^{FL/FL}$ and *Atg16l1*$^{M-KO}$ mice and quantification 0 and 36 h after PHx. (B) Representative FACS plots and quantification of MoMFs and KCs in *Atg16l1*$^{FL/FL}$ and *Atg16l1*$^{M-KO}$ mice liver tissues 0 and 36 h after PHx (n = 6 per group). (C) Representative dual IF staining for iNOS (purple) and F4/80 (green) in *Atg16l1*$^{FL/FL}$ and *Atg16l1*$^{M-KO}$ mice liver sections. Representative dual IF staining for CD206 (purple) and F4/80 (green) in liver sections 36 h post PHx compared with sham controls (n = 6 per group). (D) Representative FACS plots and quantification of Ly6C^{lo} or Ly6C^{hi} hepatic macrophages 36 h after 70% PHx (n = 6 per group). (E) Schematic of *in vitro* co-culture of primary hepatocytes with CM from sorted macrophages in *Atg16l1*$^{FL/FL}$ and *Atg16l1*$^{M-KO}$ mice. (F) Representative IF staining images of Ki67 and quantification of Ki67-positive cells in *Atg16l1*$^{FL/FL}$ and *Atg16l1*$^{M-KO}$ macrophage CM-treated hepatocytes (n = 4 per group). (G) Western blot of PCNA expression in primary hepatocytes cultured for 48 h in DMEM and the supernatant of sorted macrophages from *Atg16l1*$^{FL/FL}$ and *Atg16l1*$^{M-KO}$ mice (n = 4–6 per group). Quantitative data are also shown. (H) ELISA analysis of IL-1β, TNF-α, IL-6, and HGF secreted by sorted macrophages from *Atg16l1*$^{FL/FL}$ and *Atg16l1*$^{M-KO}$ mice (n = 6 per group). (I) Volcano plot of all DEGs in *Atg16l1*$^{FL/FL}$ and *Atg16l1*$^{M-KO}$ liver macrophages. (J) RNA-sequencing analysis of hepatic macrophages from *Atg16l1*$^{FL/FL}$ and *Atg16l1*$^{M-KO}$ mice after 70% PHx (n = 3 per group). Heatmap showing proinflammatory gene expression profiles in *Atg16l1*$^{FL/FL}$ and *Atg16l1*$^{M-KO}$ mice. (K) Quantification of mRNA expression of genes detected in (J) in *Atg16l1*$^{FL/FL}$ and *Atg16l1*$^{M-KO}$ mice. ***p <0.001, by an unpaired, 2-tailed Student's t test. Scale bars: 50 μm (C,F), 100 μm (A). ATG16L1, autophagy-related 16-like 1; CM, Conditioned medium; DEG, differentially expressed gene; IF, immunofluorescence; KO, knockout; MoMF, monocyte-derived macrophage; KC, Kupffer cell; PCNA, proliferating cell nuclear antigen; PHx, partial hepatectomy; TNF, tumor necrosis factor.

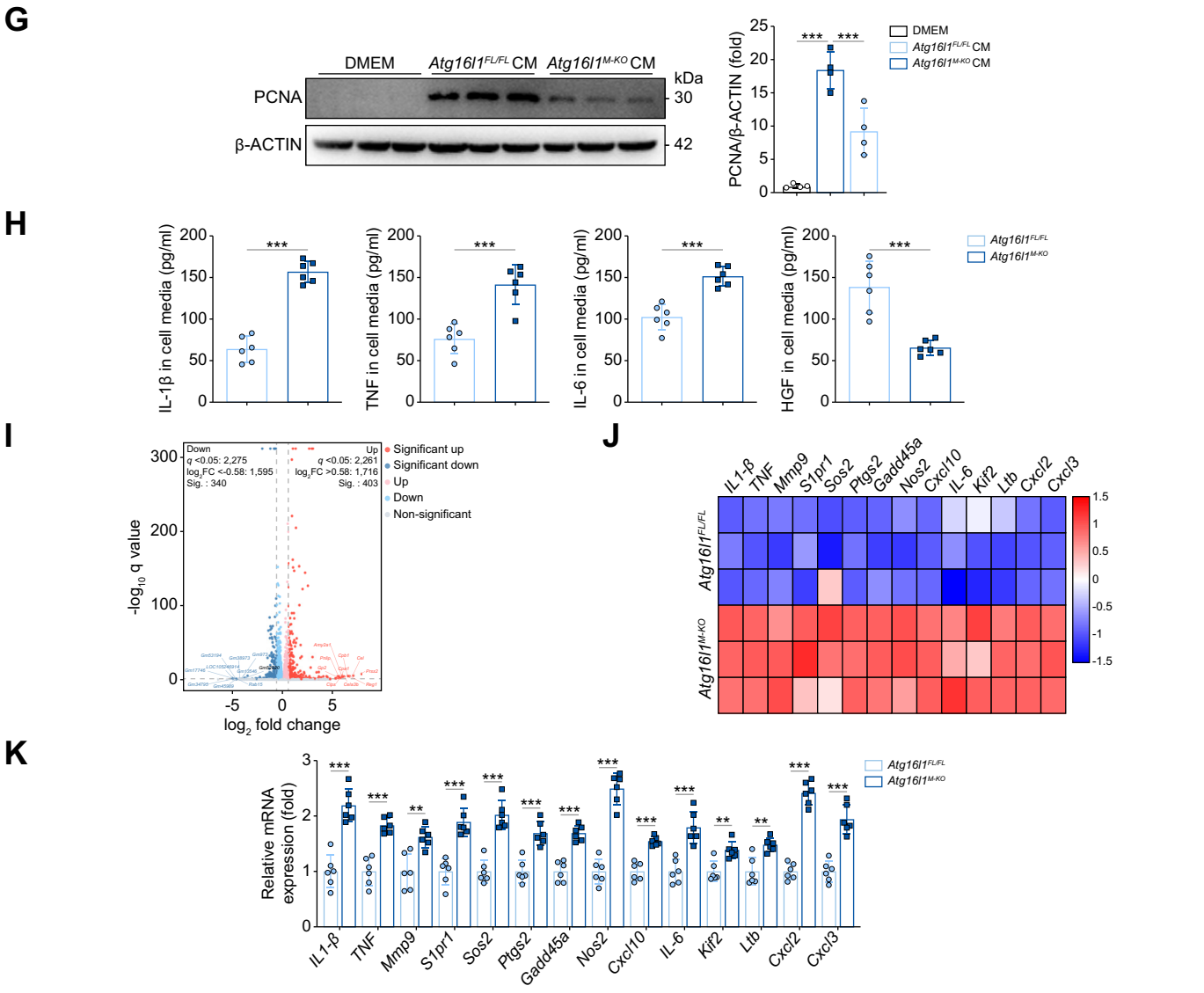

Fig. 5. (*continued*).

performed Ki67 immunohistochemical staining of liver tissue. The transfer of *Atg16l1*^{OE} macrophages significantly promoted liver regeneration in WT mice, whereas the transfer of *Atg16l1*$^{M\text{-}KO}$ macrophages had the opposite effect (Fig. 8A–D). In addition to cell therapy, we explored the effects of pharmacologically induced ATG16L1 activation on liver regeneration. After treating *Atg16l1*$^{FL/FL}$ mice with the *ATG16L1* enhancer peretinoin, we observed significant enhancement of liver regeneration (Fig. 8E,F). In conclusion, the targeted activation of ATG16L1 can effectively promote liver regeneration.

Discussion

Given that liver regeneration is a complex and dynamic process, its orderly progression requires the coordination and involvement of immune cells.[1,27] Although previous studies have thoroughly described the positive relationship between autophagy and liver regeneration, most have been limited to hepatocytes.[8,28] Therefore, our understanding of the role of autophagy in immune cells during liver regeneration remains limited. The results of this study reveal the regulatory role and mechanism of the autophagy-related gene *ATG16L1* in macrophages during liver regeneration after PHx. We demonstrated that the conditional deletion of *ATG16L1* in macrophages after PHx hinders mitophagy, leading to the accumulation of mitochondrial damage and forcing a metabolic and functional shift in macrophages from a reparative to a proinflammatory phenotype. Furthermore, ATG16L1 deficiency triggers activation of the STING signaling pathway in macrophages and inhibits its degradation, thereby reshaping the macrophage phenotype and ultimately suppressing liver regeneration. Both cell therapy and pharmacological studies suggest that the targeted activation of *ATG16L1* represents a novel strategy for promoting liver regeneration.

Effective liver regeneration is critical for a favorable clinical outcome in various liver diseases. Small-for-size syndrome is a major cause of postoperative liver failure and even death in patients undergoing liver resection or transplantation.[3] In the

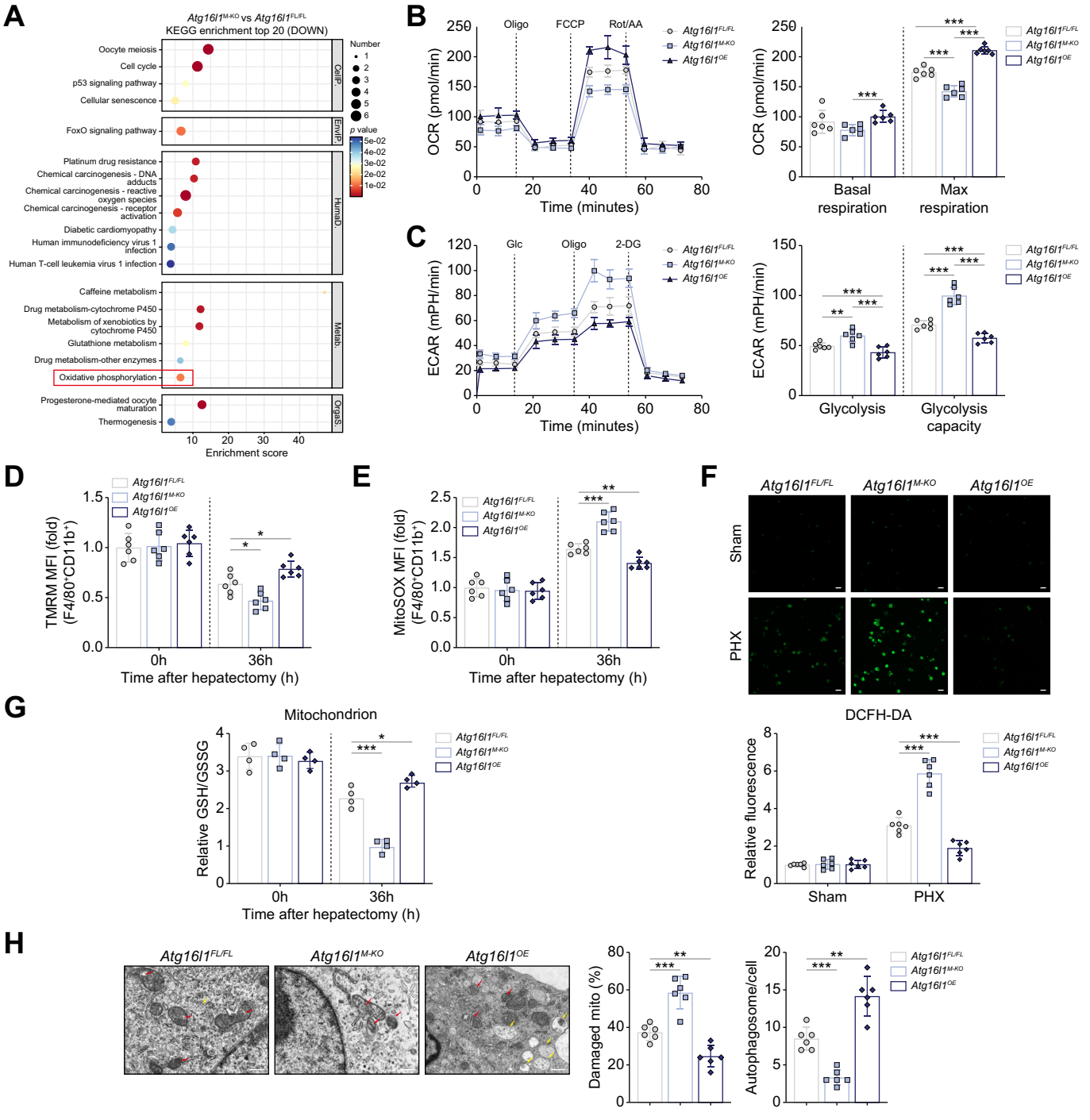

Fig. 6. ATG16L1 deletion mediates a macrophage metabolic shift by impairing mitophagy. (A) RNA-sequencing analysis of hepatic macrophages sorted by flow cytometry from mice 36 h after PHx. Bubble chart showing the top 20 significantly downregulated genes based on KEGG enrichment. The oxidative phosphorylation pathway in macrophages from *Atg16l1*$^{M\text{-}KO}$ mice had a significant *p* value. (B) OCR of macrophages sorted from *Atg16l1*$^{FL/FL}$, *Atg16l1*$^{M\text{-}KO}$, and *Atg16l1*^{OE} mice 36 h post PHx assessed by a Seahorse assay before and after the sequential addition of oligomycin, FCCP, rotenone, and antimycin (n = 6 per group). (C) ECAR assessed by a Seahorse assay of macrophages sorted from *Atg16l1*$^{FL/FL}$, *Atg16l1*$^{M\text{-}KO}$, and *Atg16l1*^{OE} mice at 36 h post PHx (n = 6 per group). $^{**}p$ <0.01,$^{***}p$ <0.001, by one-way ANOVA with Bonferroni post-test. Quantification of mitochondrial membrane potential (Δψm) (D) and mtROS levels (E) of liver F4/80 and CD11b double-positive macrophages from *Atg16l1*$^{FL/FL}$, *Atg16l1*$^{M\text{-}KO}$, and *Atg16l1*^{OE} mice 36 h post PHx (n = 6 per group). (F) Representative DCFDA fluorescence images for mtROS levels of sorted liver macrophages in *Atg16l1*$^{FL/FL}$, *Atg16l1*$^{M\text{-}KO}$, and *Atg16l1*^{OE} mice 0 and 36 h post PHx (n = 6 per group). (G) Quantification of mitochondrion GSH/GSSG levels in liver macrophages sorted from *Atg16l1*$^{FL/FL}$, *Atg16l1*$^{M\text{-}KO}$, and *Atg16l1*^{OE} mice at 0 and 36 h post PHx (n = 4 per group). (H) Representative electron microscopy images of *Atg16l1*$^{FL/FL}$, *Atg16l1*$^{M\text{-}KO}$, and *Atg16l1*^{OE} liver macrophages 36 h after PHx (n = 4 per group). Mitochondria are marked by red arrowheads, and autophagosomes are marked by yellow arrowheads. (I) Representative confocal microscopy images of liver macrophages 0 and 36 h post PHx stained with TOM20 (red) and dsDNA (green). Quantification of relative numbers of cytosolic mtDNA in macrophages from *Atg16l1*$^{FL/FL}$, *Atg16l1*$^{M\text{-}KO}$, and *Atg16l1*^{OE} mice (n = 6 per group). qPCR analysis of the mtDNA/nDNA ratio (J) and representative Western blot images of TOM20, TIM23, VDAC1, P62, LC3b, and *β*-ACTIN levels in *Atg16l1*$^{FL/FL}$, *Atg16l1*$^{M\text{-}KO}$, and *Atg16l1*^{OE} liver macrophages 36 h post PHx (n = 4–6 per group). (L) Western blot analysis of TOM20, P62, LC3B, and β-actin expression of sorted

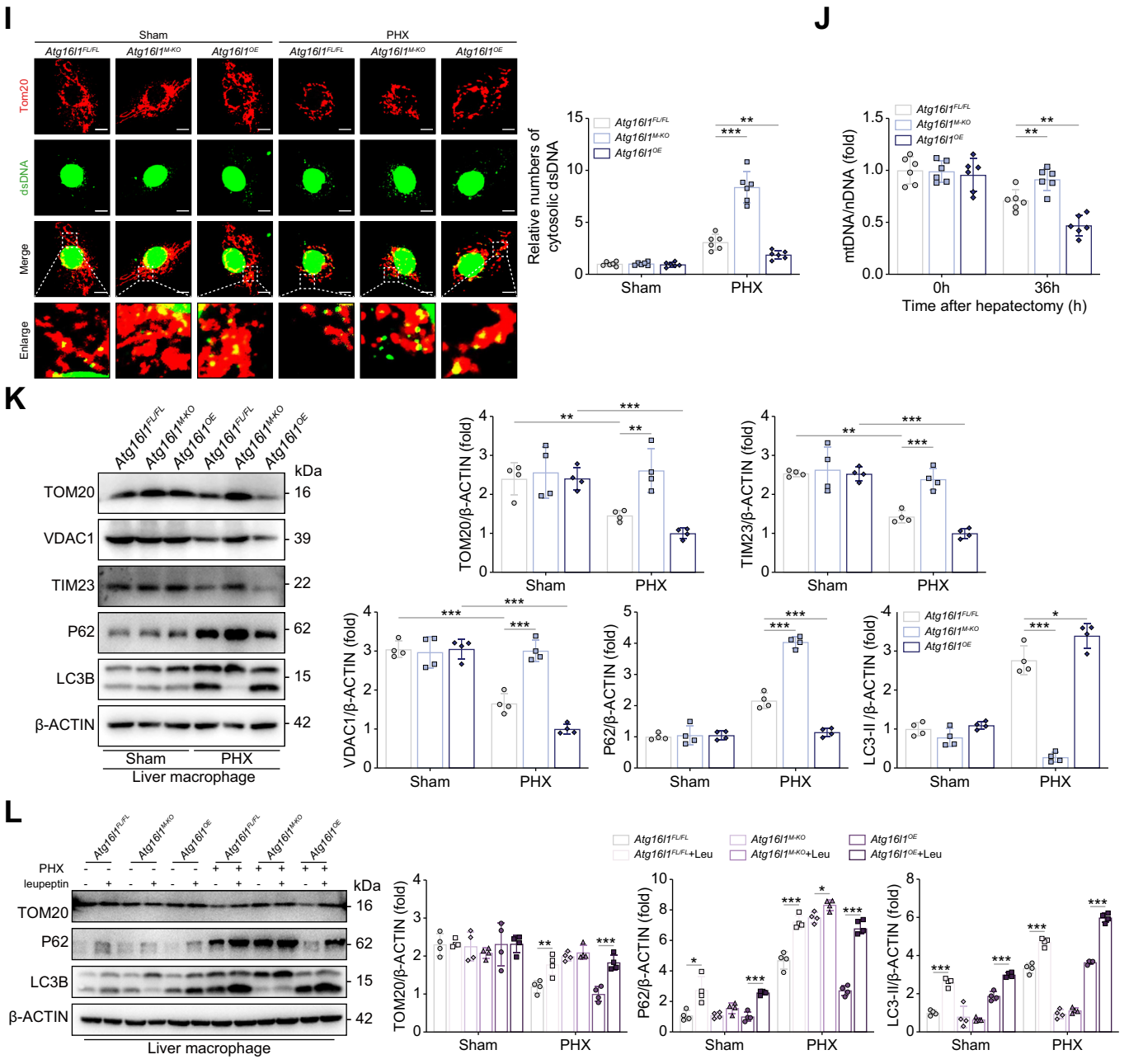

Fig. 6. (*continued*).

present study, both *Atg16l1*$^{FL/FL}$ and *Atg16l1*$^{M\text{-}KO}$ mice showed mortality in a 90% hepatectomy model. Notably, most of these mice died within 48 h post hepatectomy. Thus, early mortality in these mice may have resulted from the remnant liver volume being insufficient to provide adequate compensatory function. This would have led to significant declines in metabolic, detoxification, and digestive capacities, ultimately resulting in early death. However, the overall survival rate of *Atg16l1*$^{M\text{-}KO}$ mice was significantly lower than that of *Atg16l1*$^{FL/FL}$ mice, suggesting that differences in macrophage-mediated

macrophages in *Atg16l1*$^{FL/FL}$, *Atg16l1*$^{M\text{-}KO}$, and *Atg16l1*^{OE} mice with or without leupeptin 36 h post PHx compared with sham controls (n = 4–6 per group). *p <0.05, **p <0.01, ***p <0.001, by one-way ANOVA with Bonferroni post-test. Scale bars: 5 μm (I), 20 μm (F), 500 μm (H). ATG16L1, autophagy-related 16-like 1; ECAR, extracellular acidification rate; GSH, glutathione; GSSG, glutathione oxidized; KEGG, Kyoto Encyclopedia of Genes and Genomes; KO, knockout; Ly6C^{hi}, classically activated pro-inflammatory macrophages; Ly6C^{lo}, alternatively activated reparative macrophages; OCR, oxygen consumption rate; mtDNA, mitochondrial DNA; nDNA, nuclear DNA; ROS, reactive oxygen species; PHx, partial hepatectomy; WT, wild type.

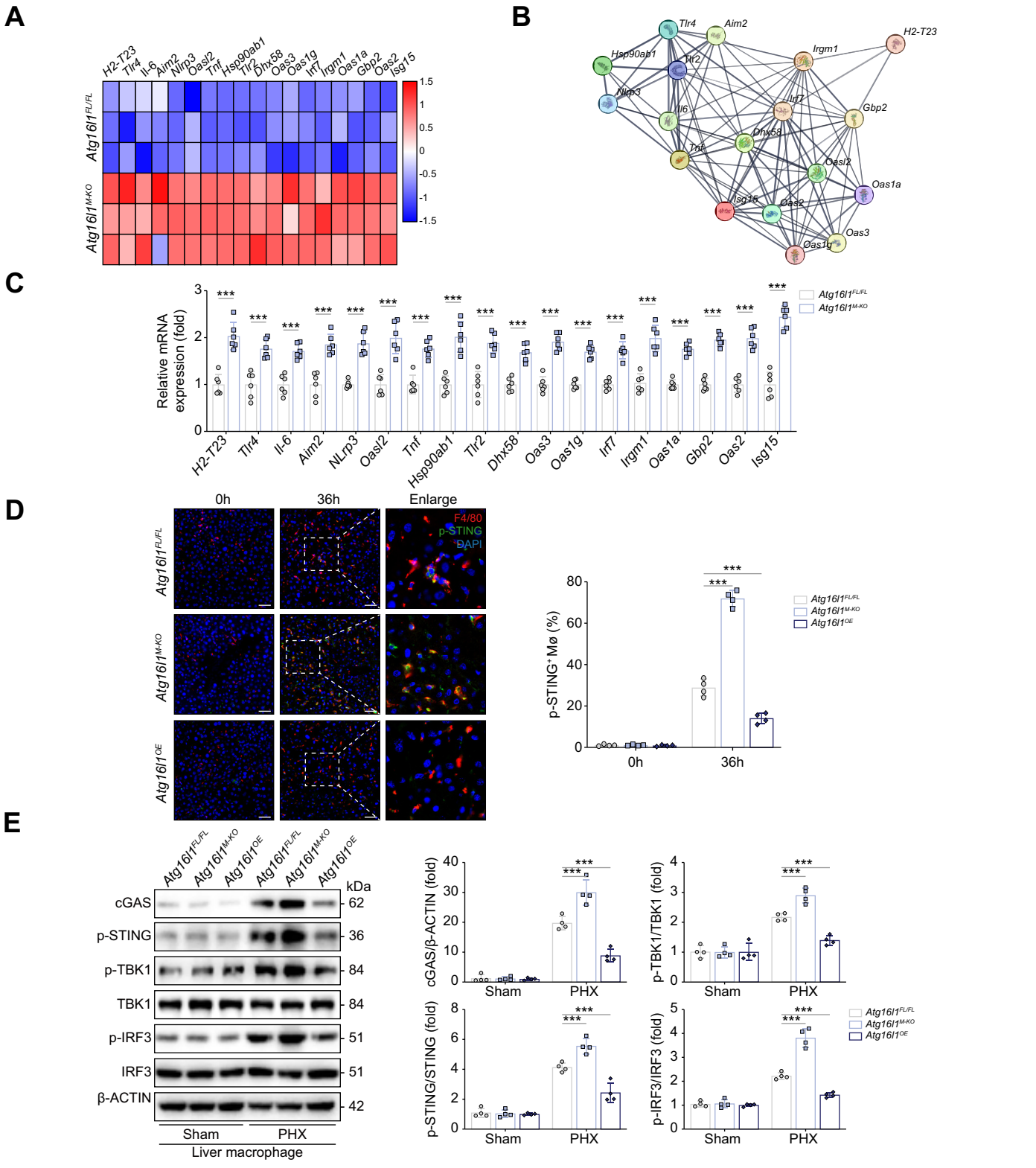

Fig. 7. Macrophage ATG16L1 deletion inhibits liver regeneration by promoting and sustaining cGAS–STING pathway activation. (A) Heatmap showing the clustering of 18 upregulated genes affecting the IFN-I response. (B) STRING-based network analysis of genes detected in (A), revealing the strong contribution of an IFN-I-related signature. (C) Quantification of mRNA expression of genes detected in (A) in *Atg16l1*$^{FL/FL}$ and *Atg16l1*$^{M-KO}$ liver macrophages. ***p <0.001, by an unpaired, 2-tailed Student's t test. (D) Representative IF co-staining images of p-STING (green), F4/80 (red), and DAPI (blue) in *Atg16l1*$^{FL/FL}$, *Atg16l1*$^{M-KO}$, and *Atg16l1*^{OE} mice 0 and 36 h after PHx. (E) Representative Western blot images of cGAS, p-STING, p-TBK1, TBK1, p-IRF3, IRF3, and β-ACTIN levels in *Atg16l1*$^{FL/FL}$, *Atg16l1*$^{M-KO}$, and *Atg16l1*^{OE} liver macrophages 36 h post PHx compared with sham controls (n = 4–6 per group). STING was silenced by AAV vectors. (F) Representative liver sections 36 and 48 h after PHx and respective quantification of Ki67-positive hepatocytes in *Atg16l1*$^{FL/FL}$+AAV-CON,

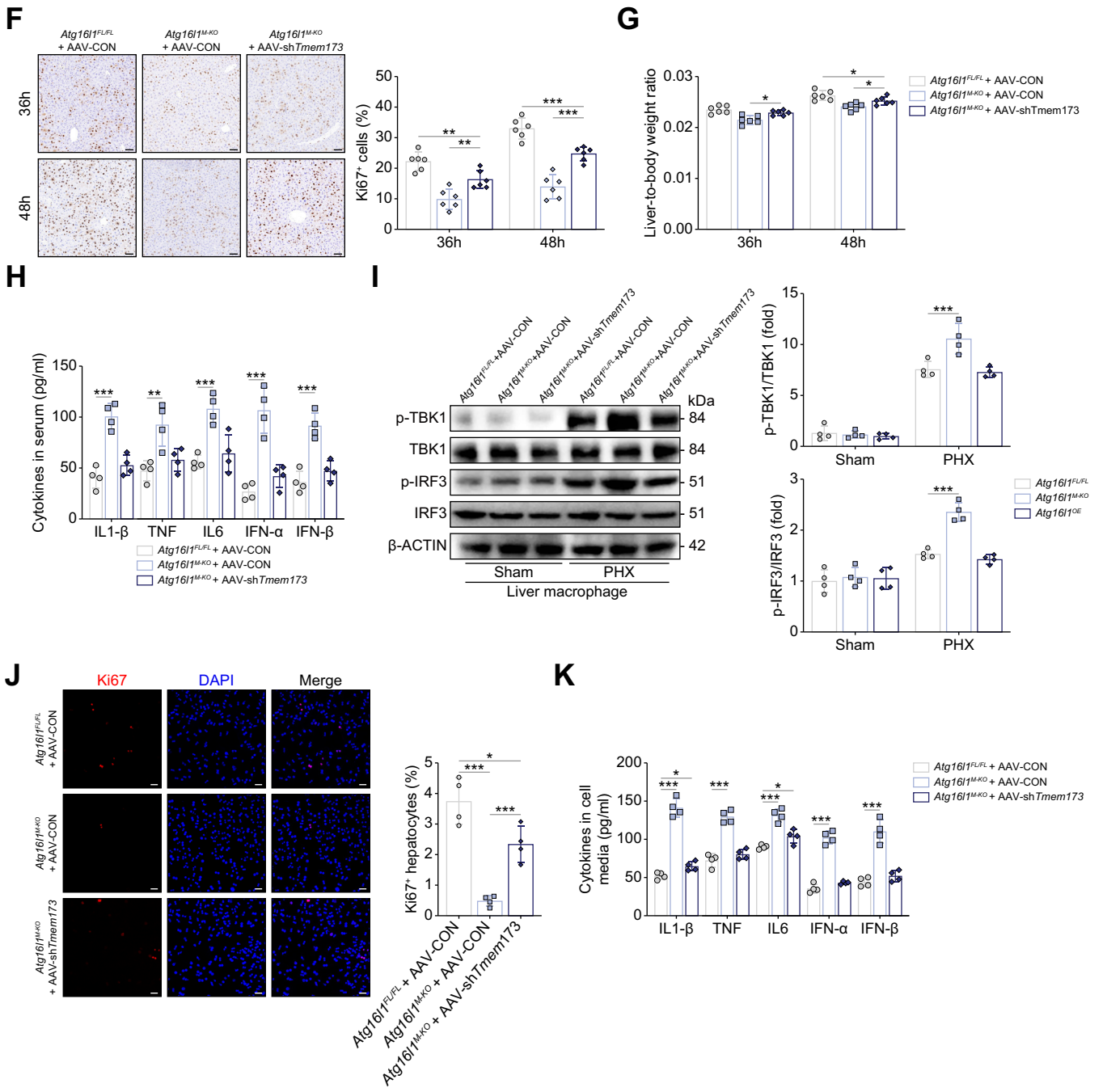

Fig. 7. (*continued*).

Atg16l1$^{M\text{-}KO}$+AAV-CON, *Atg16l1*$^{M\text{-}KO}$+AAV-sh*Tmem173* mice. Quantification of liver-to-body weight ratio 36 and 48 h after 70% PHx (G) and serum IL-1β, TNF-α, IL-6, IFN-α, and IFN-β levels assayed by ELISA 36 h post PHx (H). (I) Representative western blot images of p-TBK1, TBK1, p-IRF3, IRF3, and β-ACTIN levels in liver macrophages 36 h post PHx compared with sham controls (n = 4–6 per group). (J) Representative IF staining images of Ki67 and quantification of Ki67-positive cells in *Atg16l1*$^{FL/FL}$+AAV-CON, *Atg16l1*$^{M\text{-}KO}$+AAV-CON, *Atg16l1*$^{M\text{-}KO}$+AAV-sh*Tmem173* macrophage CM-treated hepatocytes. (K) ELISA analysis of cytokines secreted by sorted macrophages. *p <0.05, **p <0.01, ***p <0.001, by one-way ANOVA with Bonferroni post-test. Scale bars: 50 μm (D,J), 100 μm (F). AAV, adeno-associated virus; ATG16L1, autophagy-related 16-like 1; cGAS, cyclic GMP-AMP synthase; CM, conditioned medium; IF, immunofluorescence; IFN, interferon; IRF3, interferon regulatory factor 3; p-, phosphorylated; PHx, partial hepatectomy; STING, stimulator of interferon genes; TBK1, TANK-binding kinase 1; TNF, tumor necrosis factor.

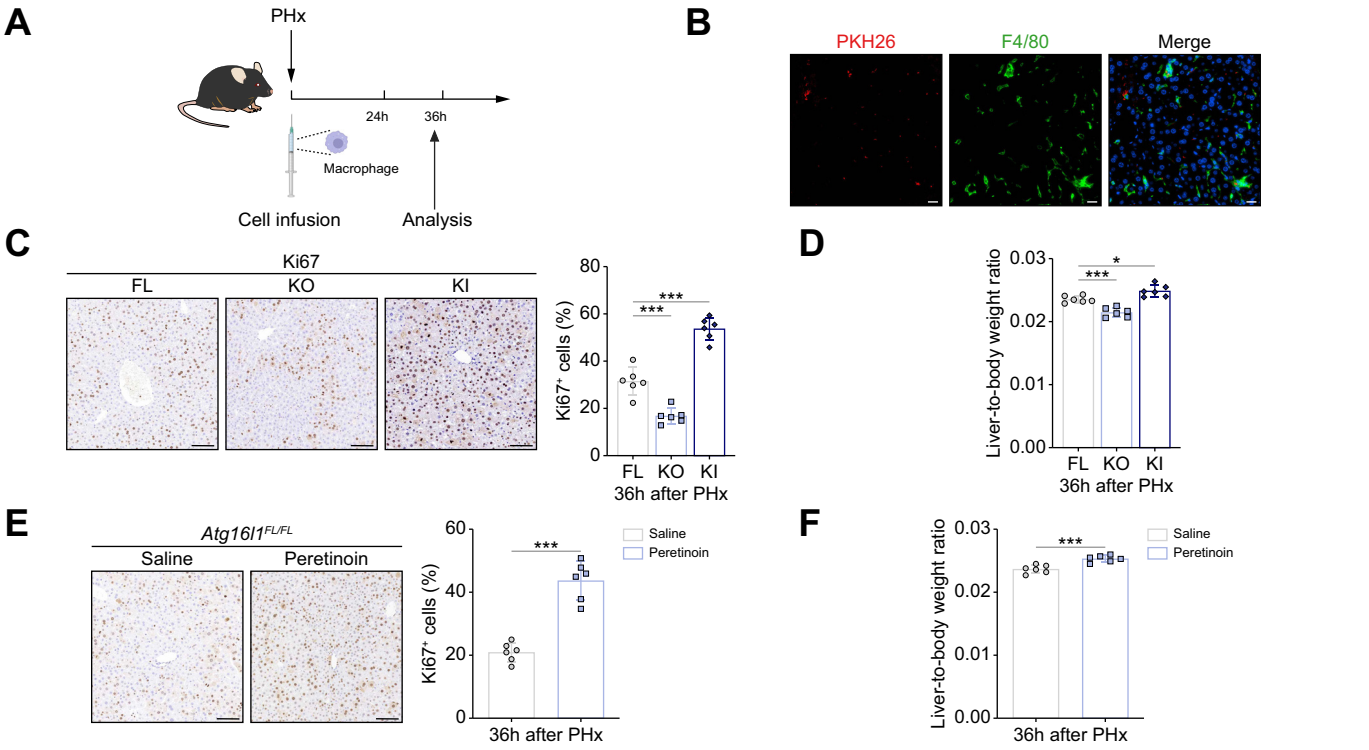

Fig. 8. Targeted activation of ATG16L1 promotes liver regeneration. (A) Strategy of BMDM infusion into mice after PHx. (B) PKH26 Dye-labeled BMDMs (red) were detected in F4/80^{+} macrophages (green) under a fluorescence microscope 36 h following cell infusion. BMDMs for infusion were sorted from *Atg16l1*$^{FL/FL}$, *Atg16l1*$^{M\text{-}KO}$, and *Atg16l1*^{OE} mice. (C) Representative liver sections 36 h after PHx and cell infusion and respective quantification of Ki67-positive hepatocytes (n = 6 per group). (D) Liver-to-body weight ratio of mice implanted with BMDMs 36 h after 70% PHx (n = 6 per group). **p* <0.05, ****p* <0.001, by one-way ANOVA with Bonferroni post-test. (E) The ATG16L1 enhancer peretinoin was used immediately after 70% PHx. Representative immunohistochemical staining images of Ki67 and quantification of Ki67-positive cells in liver sections after PHx in *Atg16l1*$^{FL/FL}$ mice. (F) Liver-to-body weight ratio of *Atg16l1*$^{FL/FL}$ mice 36 h after 70% PHx. ****p* <0.001, by an unpaired, 2-tailed Student's *t* test. Scale bars: 20 μm (B), 100 μm (C,E), ATG16L1, autophagy-related 16-like 1; BMDM, bone marrow-derived macrophage; KO, knockout; PHx, partial hepatectomy.

regeneration capacity also affect mortality. Therefore, in the 90% hepatectomy mouse model, both liver failure caused by extensive resection and aberrant macrophage-mediated regeneration regulation are likely key contributors to early mortality.

Liver regeneration is also influenced by injury factors, including the type, duration, and severity of the injury.[29] However, compared with the regeneration models induced by toxicity or drugs, liver resection is a low-injury model. In the present study, we assessed liver injury at various time points following 70% hepatectomy. We found that although alanine aminotransferase and aspartate aminotransferase levels were elevated in *Atg16l1*$^{M\text{-}KO}$ mice compared with those in the control group, liver histopathology with H&E staining showed no significant differences between the groups, indicating a relatively mild liver injury. Thus, the difference in injury caused by myeloid *Atg16l1* deficiency might not significantly affect liver regeneration. In addition, the macrophage transfusion and co-culture experiments of macrophage-conditioned medium with hepatocytes further confirmed that ATG16L1 signaling in macrophages had a crucial role in liver regeneration. Together, the delayed regeneration in *Atg16l1*$^{M\text{-}KO}$ mice might be predominantly the result of the role of macrophages during the regenerative repair phase rather than of differences in injury.

As the primary immune cell population in the liver, macrophages have a crucial role in maintaining liver homeostasis and in liver diseases.[30,31] Owing to their heterogeneity under different conditions, macrophages exhibit dual roles in disease progression. Historically, macrophages have been classified into proinflammatory M1 or anti-inflammatory M2 phenotypes; however, this classification does not apply to all scenarios.[32] Increasing attention has been given to the crucial impact of the balance between Ly6C^{hi} and Ly6C^{lo} macrophages in liver diseases.[33] During inflammatory liver injury, Ly6C^{hi} macrophages promote damage progression by secreting inflammatory mediators, such as IL-1β, IL-6, and TNF-α, whereas alternatively activated Ly6C^{lo} macrophages produce anti-inflammatory mediators, such as IL-4 and IL-10, promoting tissue repair and regeneration.[34] During liver regeneration and repair, a transition from Ly6C^{hi} to Ly6C^{lo} macrophages occurs.[35]

Liver-resident macrophages (KCs) undergo cell death in various liver disease conditions. In our previous study, we observed that KCs underwent early cell death in an acute liver ischemia–reperfusion injury model, with infiltration of peripheral macrophages into the liver, both leading to dynamic changes in the proportion of hepatic macrophages.[36] However, this study did not analyze the impact of macrophage death on liver regeneration. We quantified the absolute number of KCs and found no difference between *Atg16l1*$^{FL/FL}$ and *Atg16l1*$^{M\text{-}KO}$ mice. Therefore, the differences in macrophage proportions might be mainly the result of a significant increase in monocyte-derived macrophages following *ATG16L1* deletion. The role of

autophagy in KC death remains controversial. In a chronic intermittent hypoxia model, autophagy inhibition exacerbated KC apoptosis.[37] Conversely, autophagy inhibition significantly increased KC survival and reduced nanoparticle-induced liver damage.[38] Therefore, autophagy could have a dual role in KC death, depending on the context. Whether the liver regeneration model induces KC death and whether ATG16L1 influences KC death remains to be studied further.

Macrophage phenotype is closely linked to autophagy, with studies showing that autophagy-deficient macrophages trigger stronger inflammatory responses,[39,40] and that the M2 polarization of macrophages heavily depends on autophagy.[41] *ATG16L1*, a key autophagy gene, regulates both canonical and non-canonical autophagy by influencing LC3 lipidation.[42] Therefore, the loss of *ATG16L1* in macrophages often leads to excessive inflammation.[43] Our previous metabolic dysfunction-associated steatohepatitis model demonstrated that deletion of ATG16L1 in macrophages activated a proinflammatory phenotype, exacerbating disease progression.[10] Similarly, in the present study, Atg16l1$^{M\text{-}KO}$ mice exhibited a tendency toward proinflammatory macrophages at 36 h post PHx, with a significant decrease in reparative macrophages. This was accompanied by elevated levels of inflammatory cytokines, such as IL-1β, IL-6, and TNF-α, as well as a marked reduction in the macrophage-secreted HGF, resulting in suppressed liver regeneration. Apart from *ATG16L1*, we also detected that autophagy genes, such as *ATG5* and *ATG12*, in macrophages exhibited upregulated expression following liver resection. The involvement of hepatocyte *ATG5* in liver regeneration has been demonstrated, but further examination is warranted to elucidate its potential influence on macrophage phenotype and function during liver regenerative.

HGF secretion levels vary among macrophage populations, with Ly6C^{lo} macrophages secreting higher levels of HGF compared with Ly6C^{hi} macrophages.[17] We found that autophagy can influence HGF secretion by driving macrophage phenotype switching; following *ATG16L1* KO, liver macrophages shifted toward the Ly6C^{hi} phenotype, and HGF secretion was significantly reduced. In addition to determining macrophage phenotypes, autophagy itself may affect HGF expression. Autophagy deficiency in tumor cells can block HGF expression by inhibiting DNMT1 degradation, suggesting that HGF secretion is dependent upon autophagy.[44] However, given that autophagy often induces broad intracellular changes, multiple signaling pathways might be involved in the regulation of HGF expression by ATG16L1, warranting further investigation.

In this study, RNA-sequencing analysis revealed that macrophages with *ATG16L1* deletion had downregulated oxidative phosphorylation pathways. It is widely accepted that macrophage phenotype changes are dependent on their metabolic reprogramming. As the core of cellular metabolism, mitochondria directly influence macrophage polarization.[45] PHx can induce mitochondrial damage within cells, a phenomenon observed in hepatocytes.[8,46] However, whether PHx induces mitochondrial damage in macrophages in the regenerative environment has not been fully studied. By assessing mitochondrial function and macrophage metabolism in the liver, we found that PHx led to mitochondrial damage in macrophages, which was exacerbated by ATG16L1 deficiency, shifting their metabolism toward glycolysis. Conversely, ATG16L1 overexpression significantly improved mitochondrial function and metabolic activity.

Autophagy, particularly mitophagy, has a crucial role in regulating mitochondrial quantity and maintaining normal mitochondrial function, and is closely associated with the development of various systemic diseases.[47] Mitophagy defects in macrophages, which lead to mitochondrial damage and metabolic alterations, drive the proinflammatory transformation of macrophages.[48] Our earlier research revealed that diminished mitophagy in senescent macrophages exacerbates sterile liver inflammation.[23] However, whether mitophagy in macrophages has a protective role in mitochondria during liver regeneration has not previously been elucidated. Through further examination of mitophagy flux in macrophages, we found that ATG16L1 deletion impairs mitophagy by affecting LC3b lipidation, whereas ATG16L1 overexpression in liver macrophages enhances mitophagy, reducing mitochondrial damage. Thus, we demonstrated that ATG16L1 drives mitophagy and protects macrophage mitochondria in the liver regeneration environment. However, as a key molecule in autophagy, ATG16L1 influences other autophagy-related processes, but whether these changes also have a role in liver regeneration requires further investigation.

The cGAS–STING signaling pathway has garnered attention because of its role in antimicrobial and antitumor responses. In recent years, research identified STING as a key therapeutic target for inflammatory liver diseases, where inhibition of STING signaling effectively limits liver inflammatory damage. IFN can inhibit liver regeneration, but STING, as a key molecule in IFN activation, has not yet been fully explored in the context of liver regeneration.[24] The cytosolic release of mtDNA in macrophages can act as an intrinsic signal to activate STING in various disease models. Following PHx, we observed that mtDNA leakage in macrophages triggered STING activation, which was more pronounced in the absence of ATG16L1. Inhibiting STING signaling partially restored liver regeneration in ATG16L1-deficient mice, although the recovery was incomplete. This may be because STING inhibition cannot fully reverse mitochondrial damage in macrophages. Beyond STING activation, crosstalk exists between autophagy and STING degradation. For example, in BJ1 fibroblasts, *ATG16L1* deletion affects STING pathway protein degradation.[26] In our model, we also found that ATG16L1 deficiency inhibits the degradation of STING in macrophages.

In summary, our study highlights the crucial regulatory role of macrophage ATG16L1 signaling in liver regeneration. ATG16L1 deficiency drives metabolic reprogramming and proinflammatory polarization in macrophages by inhibiting mitophagy and simultaneously sustains excessive STING activation by both activating the pathway and inhibiting STING degradation, resulting in elevated levels of IFN and other inflammatory cytokines, thereby suppressing liver regeneration. Pharmacological activation or genetic overexpression of *ATG16L1* in macrophages significantly pro-

motes liver regeneration and repair. These findings suggest that ATG16L1 acts as a key switch for the reprogramming of macrophages into a reparative phenotype, and that the targeted activation of *ATG16L1* represents a promising new therapeutic approach for enhancing liver regeneration in clinical settings.

Affiliations

[1]*Hepatobiliary Center, The First Affiliated Hospital of Nanjing Medical University, Nanjing, 210029, China;* [2]*Key Laboratory of Liver Transplantation, Chinese Academy of Medical Sciences, Nanjing, 210029, China;* [3]*NHC Key Laboratory of Living Donor Liver Transplantation (Nanjing Medical University), Nanjing, 210029, China;* [4]*Department of Anesthesiology, Jiangsu Province People's Hospital and Nanjing Medical University First Affiliated Hospital, Nanjing, 210029, China;* [5]*Department of General Surgery, Nanjing BenQ Medical Center, The Affiliated BenQ Hospital of Nanjing Medical University, Nanjing, 210029, China*

Abbreviations

AAV, adeno-associated virus; ALT, alanine aminotransferase; AST, aspartate aminotransferase; ATG16L1, autophagy related 16-like 1 gene; BMDM, bone marrow-derived macrophage; cGAS, cyclic GMP-AMP synthase; CM, conditioned medium; DEG, differentially expressed gene; ECAR, extracellular acidification rate; GO, Gene Ontology; GSH, glutathione; HGF, hepatocyte growth factor; IF, immunofluorescence; IFN, interferon; IRF3, interferon regulatory factor 3; KC, Kupffer cell; KEGG, Kyoto Encyclopedia of Genes and Genomes; KO, knockout; Ly6C^{hi}, classically activated proinflammatory macrophages; Ly6C^{lo}, alternatively activated reparative macrophages; MoMF, monocyte-derived macrophage; mtDNA, mitochondrial DNA; mtROS, mitochondrial reactive oxygen species; nDNA, nuclear DNA; NK, natural killer; OCR, oxygen consumption rate; p-, phosphorylated; PCNA, proliferating cell nuclear antigen; PHx, partial hepatectomy; qPCR, quantitative PCR; ROS, reactive oxygen species; STAT3, signal transducer and activator of transcription 3; STING, stimulator of interferon genes; TBK1, TANK-binding kinase; TNF, tumor necrosis factor; WT, wild type.

Financial support

This study was supported by the National Natural Science Foundation of China (82370668, 82071798), Natural Science Foundation of Jiangsu Province (BK20240053), Jiangsu Science and Education Capacity Enhancement Project (ZDXYS202201, CXZX202203), and Postgraduate Research & Practice Innovation Program of Jiangsu Province (KYCX24_2030).

Conflicts of interest

The authors declare no potential conflicts of interest with respect to the research, authorship, and publication of this article.

Please refer to the accompanying ICMJE disclosure forms for further details.

Authors' contributions

XZ: study design, conducting experiments, and drafting the manuscript. YB, QZ: conducting experiments, and supplementing the manuscript.YG: acquisition of data, analysis, and interpretation of data. QB, FL: critical revision of the manuscript for important intellectual content. ZZ: technical support. ZR, HZ: study concept and design, analysis, and interpretation of data, drafting the manuscript, obtaining funding, and study supervision.

Data availability statement

Data are available on reasonable request to the corresponding authors.

Acknowledgements

We are grateful to BioRender (biorender.com) for providing diagram support.

Supplementary data

Supplementary data to this article can be found online at https://doi.org/10.1016/j.jhepr.2025.101330.

References

Author names in bold designate shared co-first authorship.

[1] Campana L, Esser H, Huch M, Forbes S. Liver regeneration and inflammation: from fundamental science to clinical applications. Nat Rev Mol Cell Biol 2021;22:608–624.

[2] Michalopoulos GK, DeFrances MC. Liver regeneration. Science 1997;276:60–66.

[3] Dahm F, Georgiev P, Clavien PA. Small-for-size syndrome after partial liver transplantation: definition, mechanisms of disease and clinical implications. Am J Transpl 2005;5:2605–2610.

[4] Tacke F, Zimmermann HW. Macrophage heterogeneity in liver injury and fibrosis. J Hepatol 2014;60:1090–1096.

[5] Wynn TA, Vannella KM. Macrophages in tissue repair, regeneration, and fibrosis. Immunity 2016;44:450–462.

[6] **Dal-Secco D**, **Wang J**, Zeng Z, et al. A dynamic spectrum of monocytes arising from the in situ reprogramming of CCR2+ monocytes at a site of sterile injury. J Exp Med 2015;212:447–456.

[7] Ramachandran P, Pellicoro A, Vernon MA, et al. Differential Ly-6C expression identifies the recruited macrophage phenotype, which orchestrates the regression of murine liver fibrosis. Proc Natl Acad Sci U S A 2012;109:E3186–E3195.

[8] Toshima T, Shirabe K, Fukuhara T, et al. Suppression of autophagy during liver regeneration impairs energy charge and hepatocyte senescence in mice. Hepatology 2014;60:290–300.

[9] **Villamuera R**, **Fernández-Cabrera A**, **Serramito-Gómez I**, et al. Unconventional WD40 domain-dependent role of ATG16L1 in the regulation of IL10R (interleukin 10 receptor) endocytosis, trafficking and signaling. Autophagy 2021;17:2639–2641.

[10] **Wang Q**, **Bu Q**, **Xu Z**, et al. Macrophage ATG16L1 expression suppresses metabolic dysfunction-associated steatohepatitis progression by promoting lipophagy. Clin Mol Hepatol 2024;30:515–538.

[11] Mitchell C, Willenbring H. A reproducible and well-tolerated method for 2/3 partial hepatectomy in mice. Nat Protoc 2008;3:1167–1170.

[12] **Ma P**, **Zhao W**, Gao C, et al. The contribution of hepatic macrophage heterogeneity during liver regeneration after partial hepatectomy in mice. J Immunol Res 2022;2022:3353250.

[13] Michalopoulos GK, Bhushan B. Liver regeneration: biological and pathological mechanisms and implications. Nat Rev Gastroenterol Hepatol 2021;18:40–55.

[14] Yin S, Wang H, Park O, et al. Enhanced liver regeneration in IL-10-deficient mice after partial hepatectomy via stimulating inflammatory response and activating hepatocyte STAT3. Am J Pathol 2011;178:1614–1621.

[15] Li N, Hua J. Immune cells in liver regeneration. Oncotarget 2017;8:3628–3639.

[16] **Yang W**, **Tao Y**, Wu Y, et al. Neutrophils promote the development of reparative macrophages mediated by ROS to orchestrate liver repair. Nat Commun 2019;10:1076.

[17] **Huang M**, **Jiao J**, **Cai H**, et al. C-C motif chemokine ligand 5 confines liver regeneration by down-regulating reparative macrophage-derived hepatocyte growth factor in a forkhead box O 3a-dependent manner. Hepatology 2022;76:1706–1722.

[18] **Jia D**, **Jiang H**, Weng X, et al. Interleukin-35 promotes macrophage survival and improves wound healing after myocardial infarction in mice. Circ Res 2019;124:1323–1336.

[19] Saha S, Shalova IN, Biswas SK. Metabolic regulation of macrophage phenotype and function. Immunol Rev 2017;280:102–111.

[20] Spinelli JB, Haigis MC. The multifaceted contributions of mitochondria to cellular metabolism. Nat Cell Biol 2018;20:745–754.

[21] Matsuzawa-Ishimoto Y, Hwang S, Cadwell K. Autophagy and inflammation. Annu Rev Immunol 2018;36:73–101.

[22] **Aden K**, **Tran F**, **Ito G**, et al. ATG16L1 orchestrates interleukin-22 signaling in the intestinal epithelium via cGAS-STING. J Exp Med 2018;215:2868–2886.

[23] **Zhong W**, **Rao Z**, Xu J, et al. Defective mitophagy in aged macrophages promotes mitochondrial DNA cytosolic leakage to activate STING signaling during liver sterile inflammation. Aging Cell 2022;21:e13622.

[24] Allaire M, Al Sayegh R, Mabire M, et al. Monoacylglycerol lipase reprograms hepatocytes and macrophages to promote liver regeneration. JHEP Rep 2023;5:100794.

[25] Szklarczyk D, Jensen LJ. Protein-protein interaction databases. Methods Mol Biol 2015;1278:39–56.

[26] Gentili M, Liu B, Papanastasiou M, et al. ESCRT-dependent STING degradation inhibits steady-state and cGAMP-induced signalling. Nat Commun 2023;14:611.

[27] **Brandel V**, **Schimek V**, Göber S, et al. Hepatectomy-induced apoptotic extracellular vesicles stimulate neutrophils to secrete regenerative growth factors. J Hepatol 2022;77:1619–1630.
[28] Enkhbold C, Morine Y, Utsunomiya T, et al. Dysfunction of liver regeneration in aged liver after partial hepatectomy. J Gastroenterol Hepatol 2015;30:1217–1224.
[29] Bhushan B, Apte U. Liver regeneration after acetaminophen hepatotoxicity: mechanisms and therapeutic opportunities. Am J Pathol 2019;189:719–729.
[30] Guilliams M, Scott CL. Liver macrophages in health and disease. Immunity 2022;55:1515–1529.
[31] Krenkel O, Tacke F. Liver macrophages in tissue homeostasis and disease. Nat Rev Immunol 2017;17:306–321.
[32] Murray PJ. Macrophage polarization. Annu Rev Physiol 2017;79:541–566.
[33] **Mabire M**, **Hegde P**, **Hammoutene A**, et al. MAIT cell inhibition promotes liver fibrosis regression via macrophage phenotype reprogramming. Nat Commun 2023;14:1830.
[34] Vannella KM, Wynn TA. Mechanisms of organ injury and repair by macrophages. Annu Rev Physiol 2017;79:593–617.
[35] Carlin LM, Auffray C, Geissmann F. Measuring intravascular migration of mouse Ly6C(low) monocytes in vivo using intravital microscopy. Curr Protoc Immunol 2013;14:14.33.1–16.
[36] **Yue S**, **Zhou H**, Wang X, et al. Prolonged ischemia triggers necrotic depletion of tissue-resident macrophages to facilitate inflammatory immune activation in liver ischemia reperfusion injury. J Immunol 2017;198:3588–3595.
[37] Li Y, Chen Y, Xiao X, et al. CX3CL1 represses autophagy via CX3CR1/CaMKII-delta/HDAC4/Rubicon axis and exacerbates chronic intermittent hypoxia induced Kupffer cell apoptosis. Cell Signal 2023;111:110873.
[38] **Zhu S**, **Zhang J**, Zhang L, et al. Inhibition of Kupffer cell autophagy abrogates nanoparticle-induced liver injury. Adv Healthc Mater 2017;6:1601252.
[39] Liu K, Zhao E, Ilyas G, et al. Impaired macrophage autophagy increases the immune response in obese mice by promoting proinflammatory macrophage polarization. Autophagy 2015;11:271–284.
[40] Lodder J, Denaes T, Chobert MN, et al. Macrophage autophagy protects against liver fibrosis in mice. Autophagy 2015;11:1280–1292.
[41] Zhu Y, Liu Y, Ma Y, et al. Macrophage autophagy deficiency-induced CEBPB accumulation alleviates atopic dermatitis via impairing M2 polarization. Cell Rep 2023;42:113430.
[42] Magné J, Green DR. LC3-associated endocytosis and the functions of Rubicon and ATG16L1. Sci Adv 2022;8:eabo5600.
[43] Symington JW, Wang C, Twentyman J, et al. ATG16L1 deficiency in macrophages drives clearance of uropathogenic *E. coli* in an IL-1β-dependent manner. Mucosal Immunol 2015;8:1388–1399.
[44] **Li J**, **Hu SB**, Wang LY, et al. Autophagy-dependent generation of Axin2+ cancer stem-like cells promotes hepatocarcinogenesis in liver cirrhosis. Oncogene 2017;36:6725–6737.
[45] Martinez J, Verbist K, Wang R, et al. The relationship between metabolism and the autophagy machinery during the innate immune response. Cell Metab 2013;17:895–900.
[46] Sato T, Yamashina S, Izumi K, et al. Cathepsin L-deficiency enhances liver regeneration after partial hepatectomy. Life Sci 2019;221:293–300.
[47] Nunnari J, Suomalainen A. Mitochondria: in sickness and in health. Cell 2012;148:1145–1159.
[48] **Patoli D**, **Mignotte F**, Deckert V, et al. Inhibition of mitophagy drives macrophage activation and antibacterial defense during sepsis. J Clin Invest 2020;130:5858–5874.

Keywords: Proinflammatory; Mitophagy; mtDNA; STING; IFN; Oxidative phosphorylation.
Received 15 September 2024; received in revised form 10 January 2025; accepted 15 January 2025; Available online 22 January 2025